1-1-2015

Modeling Roughness of Rock Discontinuity Surfaces

Christopher Pickering
University of Mississippi

MODELING ROUGHNESS OF ROCK DISCONTINUITY SURFACES

A Thesis
presented in partial fulfillment of requirements
for the degree of Master of Engineering Science
in the Department of Geology & Geological Engineering
The University of Mississippi

by

CHRISTOPHER PICKERING

May 2015

ABSTRACT

The aim of this thesis is to propose a new methodology of quantifying the rock discontinuity condition of roughness through the physically based modeling approach of signal analysis.

The development of this method came about after investigation into the use of qualitative categorizations of roughness from the RMR rating system within rock engineering system matrices. In an attempt to assign significant values to these generalized qualitative descriptions, the standard joint roughness coefficient (JRC) profiles were initially examined through basic measurements, such as aperture and ramp angle.

Following these initial measurements and identification of inconsistencies in the wave parameters of the ten standard JRC profiles, further statistical analysis was carried out on the profiles for the purposes of both clarifying the selection and ranking of these profiles as well as finding a consistent method of JRC calculation.

Based on conclusions formed from statistical analysis, signal analysis was performed on the ten standard profiles by applying the fast Fourier transform algorithm. The results from this signal analysis allowed for the comparison of profiles through the straightforward wave parameters of wavelength and amplitude and provided a basis for the development of a methodology utilizing these parameters in the evaluation of the roughness of discontinuity profiles and the calculation of JRC.

ABBREVIATIONS

RES	Rock Engineering Systems
NATM	New Austrian Tunneling Method
RMR	Rock Mass Rating
UCS	Uniaxial Compressive Strength
RQD	Rock Quality Designation
JRC	Joint Roughness Coefficient
JRC (B&C)	Back-calculated JRC values of original ten profiles from Barton and Choubey (1977)
RMS	Root Mean Square
FFT	Fast Fourier Transform

SYMBOLS

τ	Peak shear strength
σ_n	Effective normal stress
JRC	Joint roughness coefficient
JCS	Joint wall compressive strength
ϕ_b	Basic friction angle
i	Surface inclination or ramp angle
Z_2	Root mean square first derivative
SF	Structure function
R_p	Roughness profile indexes
D	Fractal dimension
r	Divider value in fractal analysis
L(r)	Total length of a profile for a given divider value
A	Amplitude from FFT spectra
f	Frequency from FFT spectra
ϕ	Phase shift angle
PRI	Profile roughness index ($\sum_{i=1}^{100} A \cdot f$)
PRI_{10}	Profile roughness index of the largest 10 $A{\cdot}f$ values ($\sum_{j=1}^{10} A \cdot f$)

ACKNOWLEDGMENTS

It is extremely necessary to acknowledge and thank the following people, without whom this thesis would have never reached completion:

My adviser, Dr. Aydin, and committee members, Dr. Zachos and Dr. Kuszmaul, for their knowledge, guidance, and cooperation with endless questions over minor details.

The Department of Geology & Geological Engineering for the overly-generous support throughout the overly-extended length of this project and the professors, instructors, and staff who provided continual assistance and opportunities: Dr. Panhorst, Mrs. Patterson, Dr. Davidson, Dr. Easson, Ms. Grace, and Mrs. Bolen.

My mom, Diane Pickering, dad, Mike Pickering, and brother, Andrew Pickering, for consistently encouraging me to begin, continue, and finish this undertaking.

Prof. B.-A. Jang of Kangwon National University (Republic of Korea) for sharing their invaluable digitized profile data sets.

My friends, office-mates, and fellow TAs for their help, input, and keeping me grounded and entertained throughout the semesters: Zhen G., Hetherington S., Richard D., Austin P., Cindy C., Scott M., Devin T., Dakota K., Charlie K., Peshani H., Michael J., Konnor H., Tucker A., Emily R., Sam Z., Ari M., Amanda C., Justin H., Chayan L., Aaron J., Lee N., Saeed A., Chris K., Tyler R., Alex W., Moones A., Sam L., Cat H., Laura M., and Gabe P.

TABLE OF CONTENTS

TABLE OF CONTENTS CONT.

LIST OF TABLES

LIST OF FIGURES

LIST OF FIGURES CONT.

I. INTRODUCTION

When classifying the rock discontinuity condition of roughness, the methods of categorization, measurement, or calculation across the devised systems can vary significantly. Rating systems for rock masses apply qualitative descriptions of roughness that correspond to particular rating values or incorporate figures of representative profiles for the purpose of visual comparison and the designation of a coefficient value characterizing a discontinuity profile's degree of roughness. Additionally, there are field methods involving the measurement of asperity amplitudes or surface inclination angles and purely statistical methods developed for use with digitized linear profile data. Although these varying methods can provide some structure in the categorization of roughness within their respective systems, the qualitative methods are extremely generalized and restrictive while the quantitative statistical methods are often difficult to interpret or under-representative of a discontinuity profile's complete physical parameters. The development of a new approach of quantifying roughness that is based on recognizable and understandable physical wave parameters rather than obscure statistical calculations or qualitative descriptions will be a substantial asset in the analysis of rock discontinuity profiles.

II. FRAMEWORK

II-a. EARLY WORK – ROCK ENGINEERING SYSTEMS

The preliminary work for this thesis began with the investigation of utilizing Rock Engineering Systems (RES) in NATM tunneling projects. The RES method was developed by John Hudson (1992) for use with geotechnical design and construction. This system uses rock mass interaction matrices in an attempt to determine the most dominant and most interactive parameters across selected geotechnical parameters for a particular project. The interaction between each set of parameters is given a rating (e.g. 0 for no interaction and 5 for a critical interaction) and then each row and column are summed to find a total cause and effect value for each parameter (Hudson, 1992).

					Cause
	Parameter 1	P1 → P2	P1 → P3	P1 → P4	∑ P1 row
	P2 → P1	**Parameter 2**	P2 → P3	P2 → P4	∑ P2 row
	P3 → P1	P3 → P2	**Parameter 3**	P3 → P4	∑ P3 row
	P4 → P1	P4 → P2	P4 → P3	**Parameter 4**	∑ P4 row
Effect	∑ P1 column	∑ P2 column	∑ P3 column	∑ P4 column	Avg. of cause & effect

Table II-1: Example interaction matrix. Px → Py indicates the effect of parameter X on Y.

Within these matrices, the *cause* (summation of each row) signifies the way that a parameter affects the whole system and the *effect* (summation of each column) signifies the effect that the system has on that parameter. These variables are then used to calculate what is termed *interactivity* and *dominance* for each of the parameters. *Interactivity* is the sum of the effects of a parameter on the system and the effects of the system on the parameters (*cause* + *effect*). *Dominance* is the comparison of how a parameter affects a system versus how the system affects that parameter (*cause* – *effect*) (Singh, 1999).

The particular objective was to explore the utility of rock mass interaction matrices in translating monitored displacements by developing an interaction matrices system that could be used with NATM tunneling projects during the construction phase across varying geo-environmental conditions. These specific interaction matrices were constructed from essential rock material parameters, discontinuity parameters, and environmental factors based on the Rock Mass Rating (RMR) system (Chapman, 2010; Pariseau, 2012). Through the use of these matrices and interpretation of the causes and effects between the selected parameters, a set of guidelines could be established linking necessary changes in excavation sequences and support components to most dominant and most interactive parameters. Based on modified RMR classification parameters, an initial matrix was developed containing the following selected parameters:

1) Uniaxial Compressive Strength (UCS)
2) Groundwater condition
3) Representative *discontinuity orientation*
4) Representative *Discontinuity Condition* parameter
5) Representative *Degree of Fracturing* parameter

						Cause
	UCS					∑ P1 row
		GW Cond.				∑ P2 row
			Disc. Orientation			∑ P3 row
				Disc. Condition		∑ P4 row
					Deg. of Frac.	∑ P5 row
Effect	∑ P1 column	∑ P2 column	∑ P3 column	∑ P4 column	∑ P5 column	Avg. of cause & effect

Table II-2: Selected parameters for initial Rock Mass Interaction Matrix for use with NATM tunneling projects.

While UCS, groundwater condition, and discontinuity orientating had more straightforward values and interactions, parameters 4 and 5 were broken down into two separate matrices based on detailed classification parameters that are more likely to have mutual influence. These two separate matrices were designed to find the most representative parameters in each category for use in the original matrix in order to avoid a large, overcomplicated matrix. The *Discontinuity Condition* (from RMR) and *Degree of Fracturing* matrices were made up of the following parameters:

Discontinuity Condition Matrix

1) Aperture
2) Roughness
3) Filling
4) Weathering

Degree of Fracturing Matrix

1) Rock Quality Designation (RQD)
2) Joint spacing
3) Persistence
4) Fracturing index
5) Number of joint sets

For these two more detailed matrices, an *influence rating* based on parameter values was determined rather than an *interaction rating*. By examining *influence*, this allowed for ratings that could change based on differing environmental conditions and parameter values (rock mass scenarios), whereas most basic parameter *interactions* would retain the same rating regardless of environmental conditions (Hudson and Harrison, 1997). For example: *influence* would ask, "How does the particular value of aperture change the effect of the particular value of filling on the discontinuity condition?" while *interaction* would just ask, "How does aperture affect filling?"

Once conditions or values were assigned to all parameters within each matrix, the interactions between all parameters were determined, and the cause and effects were summed, the results could be plotted to visually compare the dominance and interactivity of each parameter and determine the most dominant. In these plots, *cause* is plotted along the x-axis, *effect* along the y-axis, *interactivity* as the positive diagonal (from corner to corner), and *dominance* as the negative diagonal (Singh and Goel, 1999). As an example, a hypothetical tunneling project (designed as a shallow transportation tunnel in heavily faulted and jointed hard rock) produced the following data and results for the *Discontinuity Condition* matrix parameters (Fig. II-1). From these results, aperture is considered the most dominant of the four parameters used in this matrix (shown by the grey positive diagonals) based on the hypothetical conditions, the parameter values, and the influence ratings between the parameters.

Parameter A	Parameter B	Influence Rating
Aperture: 0.1-0.5 mm	Roughness: slight	2
	Filling: hard/occasional	2
	Weathering: minimal	1

Parameter A	Parameter B	Influence Rating
Filling: hard/occasional	Aperture: 0.1-0.5 mm	1
	Roughness: slight	2
	Weathering: minimal	1

					Cause
	Aperture	2	2	1	**5**
	2	**Roughness**	1	1	**4**
	1	2	**Filling**	1	**4**
	1	1	1	**Weathering**	**3**
Effect	**4**	**5**	**4**	**3**	Average: 4

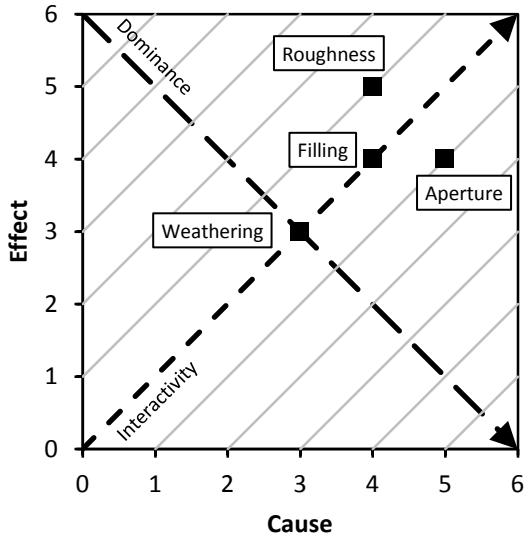

Figure II-1: Hypothetical example of conditions/values for *Discontinuity Condition* matrix.

II-b. ROUGHNESS CLASSIFICATION – JOINT ROUGHNESS COEFFICIENT

After the basic structure for the matrices had been established, an attempt was made to better quantify many of the parameters for more efficient and accurate influence/interaction determination between them. This began with converting measured values for each of the parameters to normalized scales, ranking each from least ideal (0) to most ideal (1). For parameters such as those in the *Degree of Fracturing* matrix which have quantifiable values (and in many cases, pre-determined ranges such as in RMR), this was relatively easily accomplished. However, for parameters such as roughness, filling, or weathering, which use qualitative descriptions in RMR (e.g. slightly rough, hard filling, minimal weathering), this was challenging and not straightforward. This issue with incompatible measurement normalizing led to the examination of alternate methods which have been developed for the purpose of quantifying these rock mass parameters.

The discontinuity condition *roughness* is qualitatively described for different ratings in the RMR and Q systems (e.g. very rough, rough, slightly, rough, smooth, slickensided) (Goodman, 1989; Chapman, 2010). However, other methods have been developed in order to quantify this discontinuity condition.

Presently, one of the most widely used methods, originally proposed by Barton (1973) and further developed by Barton and Choubey (1977), contains a set of ten standard joint roughness profiles. These profiles represent the full range of joint roughness coefficient values (ranging from 0 for an extremely smooth profile to 20 for an extremely rough profile). By visually comparing a discontinuity surface with these ten standard roughness profiles, a JRC value can be obtained for use in the Rock Mass Quality Rating system and peak shear strength calculations.

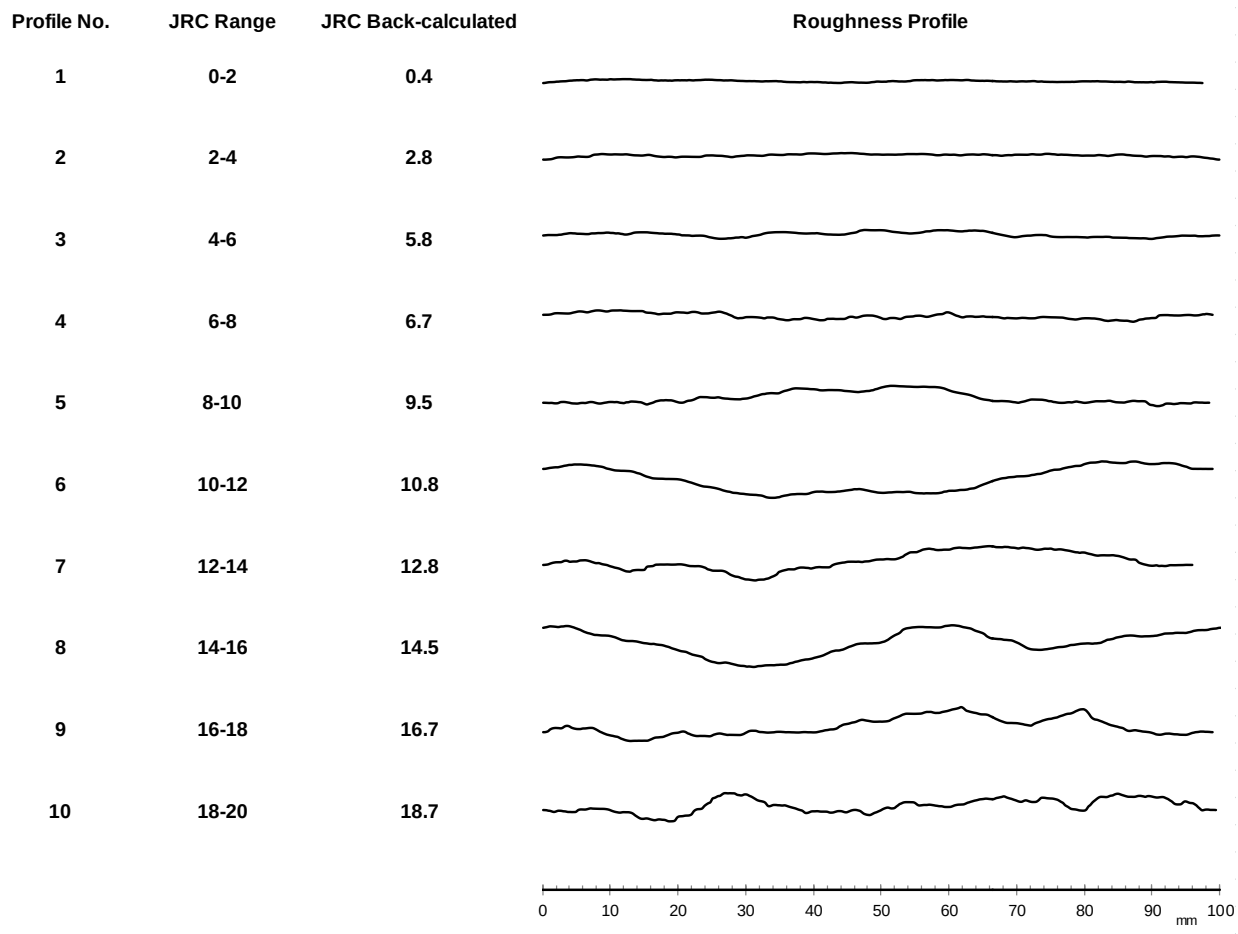

Figure II-2: The original ten standard roughness profiles selected by Barton and Choubey (1977) with representative JRC ranges and back-calculated JRC values.

II-c. PEAK SHEAR STRENGTH CALCULATION

The roughness of a rock discontinuity surface will have a direct influence on that surface's peak shear strength and therefore its resistance to failure in the shear plane. JRC values can be used within an empirical relationship developed by Barton (1973), making accurate prediction of this factor a critical component of rock discontinuity characterization in geotechnical engineering stability analysis.

$$\tau = \sigma_n \tan\left(JRC \log_{10}\left(\frac{JCS}{\sigma_n}\right) + \phi_b\right)$$ (Barton and Choubey, 1977)

where

	τ	Peak shear strength
	σ_n	Effective normal stress
	JRC	Joint roughness coefficient
	JCS	Joint wall compressive strength
	ϕ_b	Basic friction angle

Barton and Choubey (1977) state that this equation can serve three varying uses: 1) curve fitting to experimental peak shear strength data; 2) extrapolation of experimental peak shear strength data; and 3) prediction of peak shear strength. These varying uses are possible due to the ability to interpolate the values of many of the constants within common limits based on rock types and weathering conditions (e.g. ϕ_b = 25°-35°) or through estimation from simple index tests (e.g. *JCS* through Schmidt hammer rebound tests). To obtain a specific JRC number for each profile (Fig. II-2), back-calculation of the peak shear strength equation was performed after shear tests were completed on each profile sample.

$$JRC = \frac{arctan(\tau/\sigma_n) - \phi_b}{\log_{10}(JCS/\sigma_n)}$$ (Barton and Choubey, 1977)

III. PRELIMINARY ANALYSIS OF JRC

III-a. APERTURE

Preliminary analysis of the JRC system involved two-dimensional digitization and measurement of the ten standard profiles developed by Barton and Choubey (1977). All ten profiles were first traced and digitized using image editing software and designated as "bottom" joint surfaces, then perfectly matching "top" surface profiles were copied and created. These top surface profiles were moved in intervals of +/- 5 mm right and left from the center point up to a maximum of +/- 50 mm (for a total of 20 locations for each profile) and then moved upward until the top and bottom profile lines did not intersect or cross-over one another but at least one point of contact still existed. Through this method, 200 "discontinuity surfaces" were created (each spanning a linear length of 50 mm), which could be used in digital analysis and measurement. Using the image editing software, the total open areas between the top and bottom surfaces were digitized and measured for each of the 200 discontinuity surfaces (Fig. III-1a and III-1b).

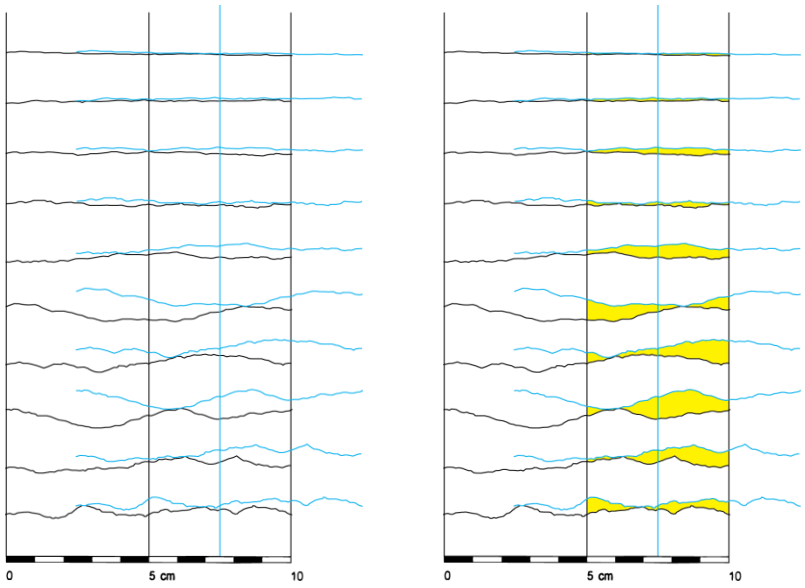

Figure III-1a: Upper discontinuity surfaces shifted +25 mm with measured aperture areas.

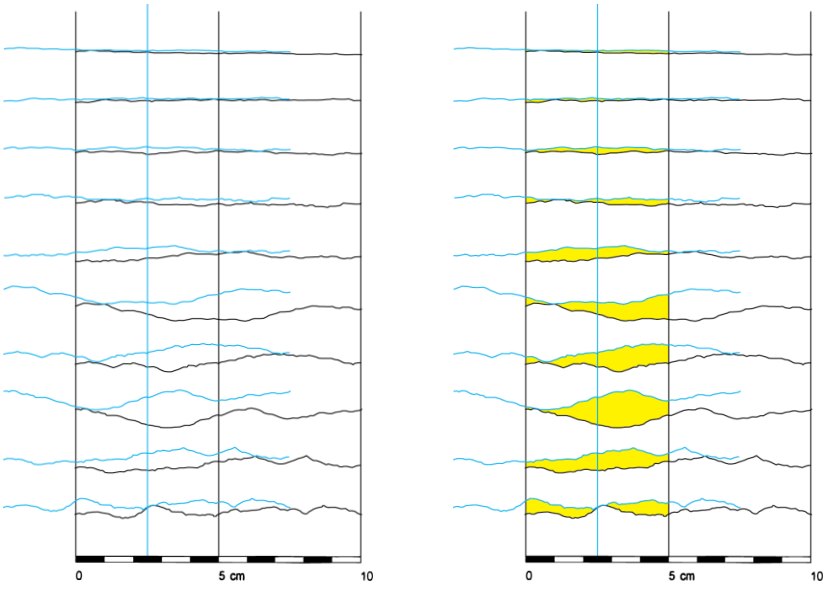

Figure III-1b: Upper discontinuity surfaces shifted -25 mm with measured aperture areas.

With these measured areas (Table III-1) for each discontinuity surface, the average aperture was calculated for each surface using the equation $\frac{area\ (mm^2)}{50\ mm}$ (Table III-2). This average aperture value across all 20 locations for each of the ten original standard profiles was plotted for an initial comparison of the profiles (Fig. III-2).

		Profile#									
		1	**2**	**3**	**4**	**5**	**6**	**7**	**8**	**9**	**10**
Displ. (mm)	**-50**	34	44	61	49	124	308	168	225	203	177
	-45	36	33	43	68	131	278	191	279	247	134
	-40	37	31	74	66	165	250	253	367	281	115
	-35	35	35	65	84	181	260	249	379	313	137
	-30	26	34	74	86	156	237	256	376	298	164
	-25	33	31	70	68	156	212	243	341	234	161
	-20	26	40	61	73	170	160	199	280	223	219
	-15	31	35	61	62	141	108	194	215	265	192
	-10	24	46	62	51	137	84	160	170	213	175
	-5	20	39	45	59	77	80	101	91	128	110
	5	31	55	47	60	61	87	98	97	114	163
	10	23	54	59	58	99	88	126	158	157	207
	15	24	44	65	51	121	126	137	205	159	170
	20	19	32	60	56	143	140	148	225	186	132
	25	21	40	86	51	170	172	189	246	168	129
	30	17	43	58	57	159	159	188	247	171	115
	35	17	52	76	52	159	160	199	213	181	88
	40	25	49	73	62	151	161	195	150	154	114
	45	14	57	43	56	154	217	167	92	142	111
	50	27	45	53	84	142	252	161	145	174	127
	AvgArea (mm^2)	**26.0**	**42.0**	**61.8**	**62.7**	**139.9**	**177.0**	**181.1**	**225.1**	**200.6**	**147.0**

Area in mm^2

Table III-1: Calculated area for each upper surface displacement location and average area for each profile.

		Profile #										
		1	**2**	**3**	**4**	**5**	**6**	**7**	**8**	**9**	**10**	
Displ. (mm)	**-50**	0.68	0.88	1.22	0.98	2.48	6.16	3.36	4.50	4.06	3.54	**Aperture in mm**
	-45	0.72	0.66	0.86	1.36	2.62	5.56	3.82	5.58	4.94	2.68	
	-40	0.74	0.62	1.48	1.32	3.30	5.00	5.06	7.34	5.62	2.30	
	-35	0.70	0.70	1.30	1.68	3.62	5.20	4.98	7.58	6.26	2.74	
	-30	0.52	0.68	1.48	1.72	3.12	4.74	5.12	7.52	5.96	3.28	
	-25	0.66	0.62	1.40	1.36	3.12	4.24	4.86	6.82	4.68	3.22	
	-20	0.52	0.80	1.22	1.46	3.40	3.20	3.98	5.60	4.46	4.38	
	-15	0.62	0.70	1.22	1.24	2.82	2.16	3.88	4.30	5.30	3.84	
	-10	0.48	0.92	1.24	1.02	2.74	1.68	3.20	3.40	4.26	3.50	
	-5	0.40	0.78	0.90	1.18	1.54	1.60	2.02	1.82	2.56	2.20	
	5	0.62	1.10	0.94	1.20	1.22	1.74	1.96	1.94	2.28	3.26	
	10	0.46	1.08	1.18	1.16	1.98	1.76	2.52	3.16	3.14	4.14	
	15	0.48	0.88	1.30	1.02	2.42	2.52	2.74	4.10	3.18	3.40	
	20	0.38	0.64	1.20	1.12	2.86	2.80	2.96	4.50	3.72	2.64	
	25	0.42	0.80	1.72	1.02	3.40	3.44	3.78	4.92	3.36	2.58	
	30	0.34	0.86	1.16	1.14	3.18	3.18	3.76	4.94	3.42	2.30	
	35	0.34	1.04	1.52	1.04	3.18	3.20	3.98	4.26	3.62	1.76	
	40	0.50	0.98	1.46	1.24	3.02	3.22	3.90	3.00	3.08	2.28	
	45	0.28	1.14	0.86	1.12	3.08	4.34	3.34	1.84	2.84	2.22	
	50	0.54	0.90	1.06	1.68	2.84	5.04	3.22	2.90	3.48	2.54	
	AvgApt (mm)	**0.52**	**0.84**	**1.24**	**1.25**	**2.80**	**3.54**	**3.62**	**4.50**	**4.01**	**2.94**	

Table III-2: Calculated aperture for each upper surface displacement location and average aperture for each profile.

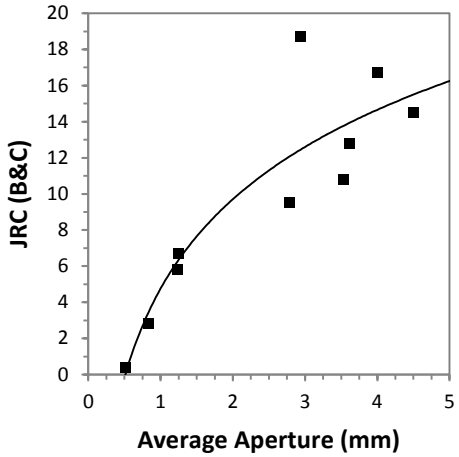

Figure III-2: Average aperture of each joint roughness profile. JRC (B&C) refers to the specific values for each profile back-calculated by Barton and Choubey (1977) (see Fig. II-2)

From observation of the plot of average apertures of each profile (Fig. III-2), it is already apparent that there is not a distinct pattern across the profiles as roughness increases. Profiles 4 and 7 stand out as points where aperture only slightly increases from the values of previous profiles and, most notably, profiles 9 and 10 actually decrease in aperture after an increase across all profiles from 1 to 8. Plotting the aperture of all 200 hypothetical discontinuity surfaces further shows the many inconsistencies and lack of patterns found across the ten roughness profiles (Fig. III-3). Two groupings of profiles can be seen between profiles 1, 2, 3, and 4 and profiles 6, 7, 8, 9, and 10, indicating a lack of consistency between the profile pattern selection, and within these groupings the lines representing each profile appear almost randomly ordered. Some crossing of the points across the 20 profile locations should be expected, but if the original roughness profiles were selected in a consistently ranked manner, the same relative order of profiles should be seen reflected in this plot. In the bottom grouping, there are multiple crossings of the profile 1 and 2 lines and the profile 3 and 4 lines that prevent a very distinct order from being interpreted, although the profile 1 and 2 lines are generally lower than those of profiles 3 and 4. In the top

grouping, only profiles 5, 7, and 8 show a mostly consistent and expected order. Profiles 6, 9, and 10 vary dramatically and without a consistent order between themselves or the other profiles. One expected pattern that the top profiles show is the general decrease in aperture as they approach the center point where the top and bottom profiles would perfectly align with no value of aperture.

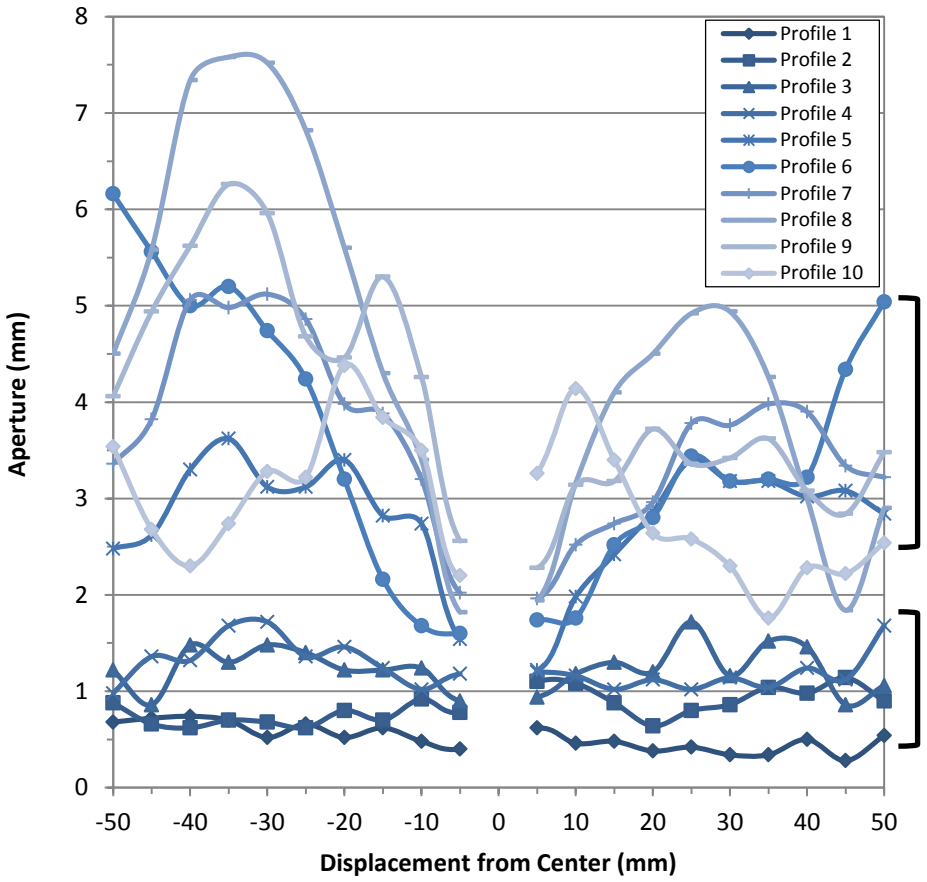

Figure III-3: Displacement of each discontinuity surface from center and aperture value at that location for resulting surface. Brackets indicate observed grouping of profiles.

III-b. MATCH & MISMATCH

After acquiring values for area and aperture, a simple equation was developed to calculate the degree of match or mismatch between the top and bottom joint surfaces. This equation calculates the departure from average aperture for each of the discontinuity surfaces.

$$\left(\frac{Aperture_{measured}}{Aperture_{average}}\right)$$

Match is shown by numbers ranging from 0 – 1 with numbers closer to 0 indicating a better match and 0 indicating a perfect match with no aperture. Mismatch is shown by numbers ranging from 1 – 2. Numbers further from 1 and closer to 2 indicate a greater mismatch and larger aperture. These match and mismatch values can help to give an indication about what might be expected for relative values of shear stresses for different roughness profiles and discontinuity surfaces. With match values closer to 0, you can expect more points between the top and bottom joint surfaces to either already be in contact or to be more likely to come into contact upon shear movement, increasing shear stresses. Higher mismatch values, indicating a worse match, will imply a surface where fewer points would be expected to be in contact or come into contact upon movement, lowering potential shear stresses. Plotting these values of match and mismatch for each of the 200 discontinuity surfaces again shows the inconsistency of wave parameters found in the ten standard joint roughness profiles (Fig. III-4).

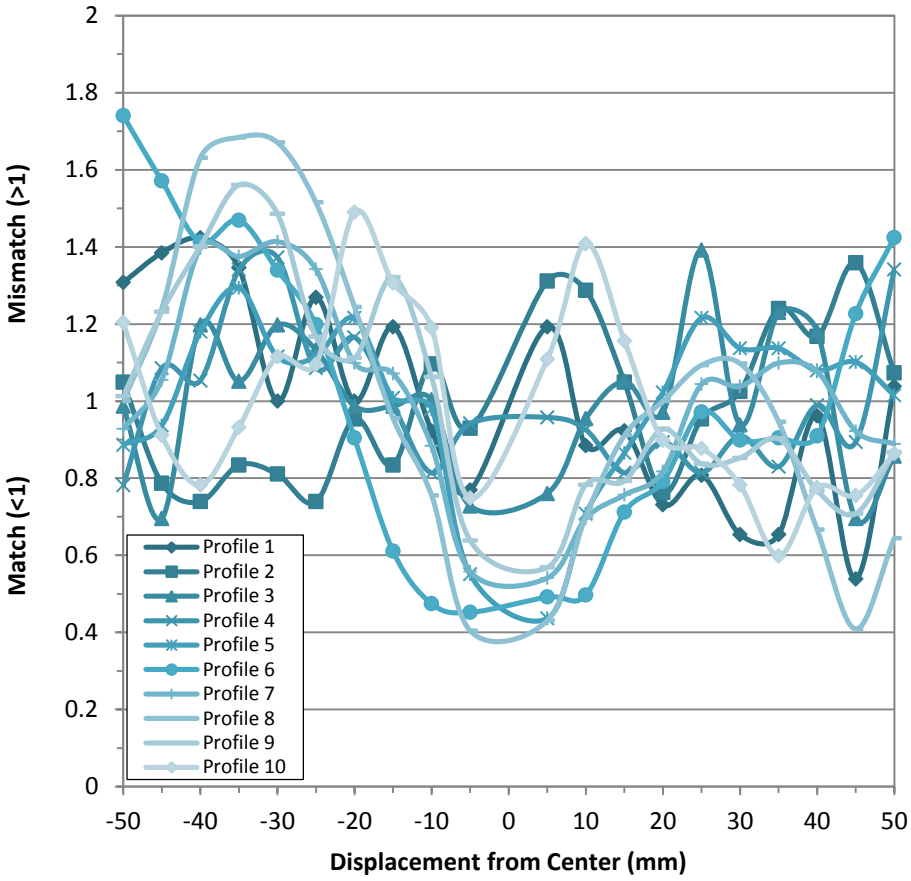

Figure III-4: Degree of Match or Mismatch for each discontinuity surface. Match values between 0-1. Mismatch values between 1-2.

Similar to Figure III-3 (Displacement vs Aperture), no specific patterns across profiles immediately stand out within the Match or Mismatch plot. However, although the profiles are again crossing and mixed, this is to be expected due to the way the values are calculated individually for each profile, where all values should center around an average of 1. Looking at each profile separately, one specific pattern can be identified that indicates an ideal standard joint roughness profile with consistent wave parameters. This pattern is the clear undulation of the line as it's traced across the plot, caused by consistently increasing and decreasing values of match

(or decreasing and increasing values of mismatch) as the top joint surface "rides" over the bottom joint surface as it is shifted at the +/- 5 mm intervals. A cleaner and more consistent undulation pattern will indicate a consistent roughness pattern across the entire joint roughness profile. This pattern is seen most clearly in profiles 1, 3, and 4, and to a lesser extent profile 2. Some undulation patterns can be seen in profiles 5-10, but they show very large and/or inconsistent wavelengths and amplitudes compared to profiles 1-4, signifying inconsistent roughness patterns and wave parameters in these standard joint roughness profiles. Ideally, with consistent profile patterns, the wavelengths and amplitudes of the undulations of each profile line on the plot should be similar, since the match and mismatch values are calculated as a percentage of the average aperture for each profile individually (e.g. 0.6 = 60% of average, 1.0 = 100% of average, 1.4 = 140% of average). All match/mismatch values would fall within a particular range (e.g. +/- 0.3) and peaks would repeat at relatively consistent intervals across the 100 mm span. With a perfectly designed synthetic profile, you could expect the undulations to alternate above and below a value of 1 with perfectly consistent wavelengths, but this would not be a realistic representation of a real-world discontinuity surface.

III-c. ROOT MEAN SQUARE

The calculation of Root Mean Square (RMS) for each of the ten standard JRC was the next preliminary background analysis performed. RMS is the square root of the mean of the squares of height values along the profiles and represents the quadratic mean magnitude (or mean amplitude) of that profile. An example of RMS calculation for a basic sine wave can be seen in Figure III-5.

$$RMS = \sqrt{(X1^2 + X2^2 + X3^2 + \cdots + Xn^2)/N}$$

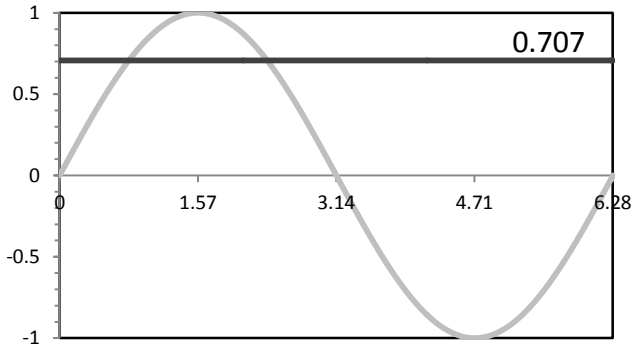

Figure III-5: Example of RMS for a basic sine wave. (RMS = 0.707)

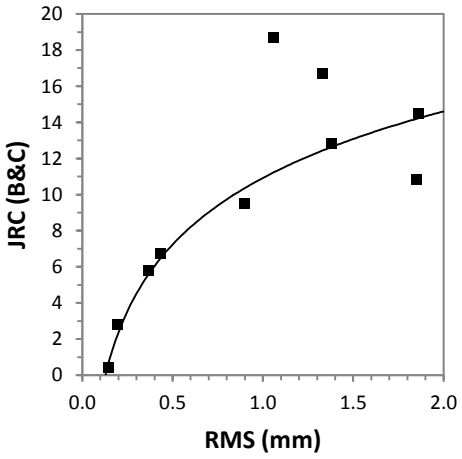

Figure III-6: RMS values of the ten standard JRC profiles from Barton and Choubey (1977).

As seen in Figure III-6, profiles 1-5, 7, and 8 fit a trend relatively well but profiles 6, 9, and 10 appear to completely ignore this trend. This result is very similar to that from the previous average aperture analysis where profiles 6, 9, and 10 fell outside the general trend that the other profiles displayed with average aperture values and where values for profiles 9 and 10 subsequently decreased after profile 8. Although RMS does not take wavelength into account, the results show the inconsistent pattern and scaling of amplitudes across the ten standard JRC profiles.

Similar to aperture, it might generally be expected for amplitude (and RMS) to increase as the roughness of a profile increases. However, through later analysis, it was seen that the range of possible RMS values increases as roughness increases due to the increasing complexity of possible constituent wave combinations. For example, between two profiles with the same statistical roughness value: one profile could have higher amplitude constituent waves at lower frequencies and lower amplitude constituent waves at higher frequencies, resulting in a higher RMS, while the other profile could have lower amplitude constituent waves at lower frequencies and higher amplitude constituent waves at higher frequencies, resulting in a lower RMS value (Fig. III-7). The statistical roughness values of the following profiles were calculated using methods in the following "*Statistical analysis"* section.

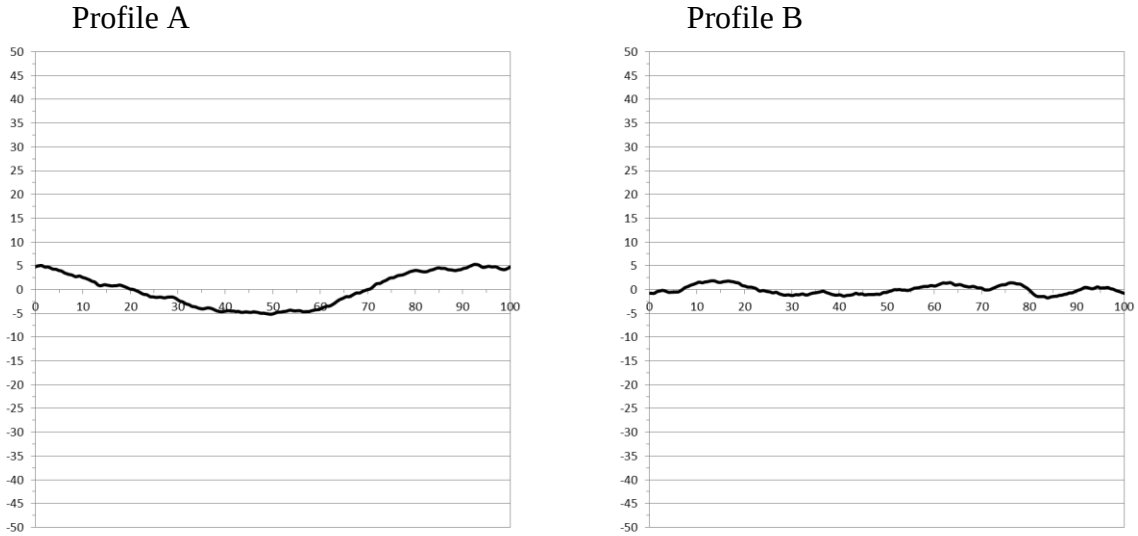

Figure III-7: Visual differences in two profiles with the same statistical roughness values. Profile A will have a higher RMS value (~3.5 mm) than Profile B (~1.4 mm).

III-d. ALTERNATE FIELD ESTIMATION METHOD

Barton (1982) proposed an alternate method for estimating JRC in the field based on his observation that an increase in the amplitude of asperities in a discontinuity profile can be related to an increase in that profile's JRC value. Rather than direct visual comparison to the ten standard profiles, a measurement can be made of the asperity amplitude of a discontinuity surface. This is accomplished by placing a straight edge along the highest points of the profile and then measuring the distance between the straight edge and the lowest point between the two peaks. With the plot proposed by Barton (1982) (Fig. III-8), this asperity amplitude measurement and the measurement of the length of the profile can be used to roughly determine the JRC for a profile. However, similar to RMS, this method does not take into account the wavelengths of asperities and the estimation of asperity amplitude is complicated with natural discontinuity surfaces (and the standard profiles) where the highest peaks are often at significantly uneven levels. The results from performing this method on the ten standard profiles can be seen in Figure III-9 and reflect the results from previous methods with the higher JRC profiles appearing out of order (with decreasing values in profiles 9 and 10) in addition to a sudden increase in asperity amplitude in profile 6, again showing the lack of consistent amplitude scaling across the profiles, despite Barton's (1982) basis for this alternate field estimation method of JRC.

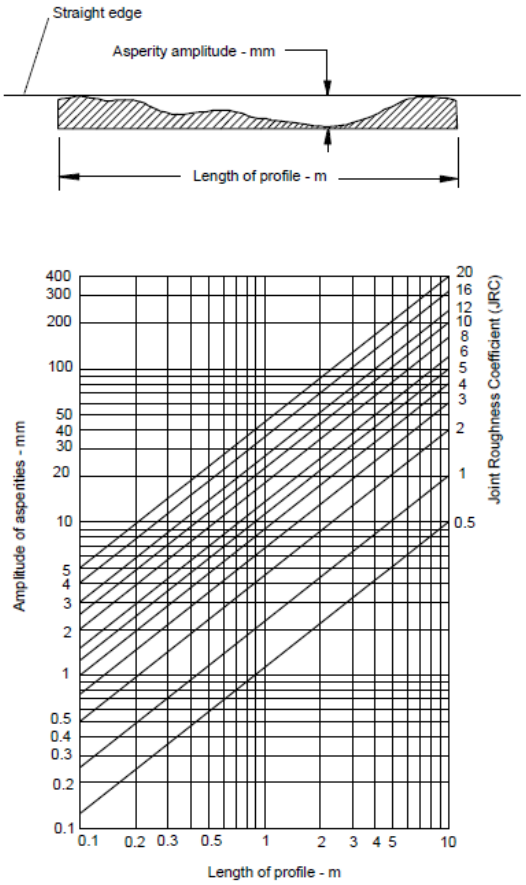

Figure III-8: Alternative field method for estimating JRC (from Barton, 1982).

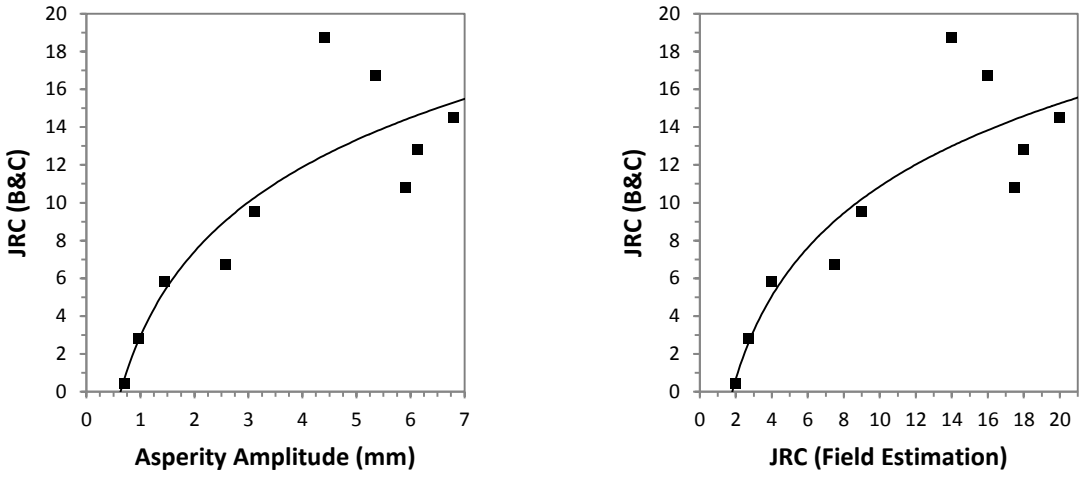

Figure III-9: Results of alternative field JRC estimation method on the ten standard profiles.

III-e. MAXIMUM RAMP ANGLE ESTIMATION

It was demonstrated by Patton (1966) that a joint friction angle of a discontinuity surface will be equal to $\phi_b + i$ (where ϕ_b is basic friction angle and i is the surface inclination or ramp angle) for simplified joint surfaces containing identical asperities oriented at an angle i from the normal plane. Values for ϕ_b generally fall between $20^o - 40^o$, with some outliers, such as sheet silicate minerals or when clay filling is present, and values for i range from $0^o - 50^o$ in the majority of cases (Goodman, 1989). Building off of this, work was done by Rengers (1970) on irregular discontinuity surfaces. Using Rengers' analysis method, a plot can be created for a discontinuity profile which shows the maximum ramp angle i between two points at varying base distance lengths, which are measured along the entire profile. Ramp angles will reach their maximum as base distances shorten and as base distances approach the full length of the profile, the ramp angle will approach 0^o. Within the plot, the positive ramp angle values represent the maximum envelope for shearing of the top surface to the right and the negative ramp angle values represent the maximum envelope for the shearing of the top surface to the left.

This analysis method was performed on the ten standard profiles to compare their maximum ramp angles, giving more insight the profile patterns and their associated wave properties. Ramp angles between points were measured at base distances of 1, 5, 10, 15, 20, 25, 30, 35, 40, 45, and 50 mm along each profile (Fig. III-10). In general, each profile shows relatively similar ramp angle (i) values in the positive and negative direction at each base distance, with the highest variation at shorter base distances. Although ramp angle values scale relatively well as profile roughness increases, the profiles with dominant longer wavelengths (6, 7, and 8) show much higher ramp angle values at longer base distances. As with previous analysis methods, these ramp angle values for profiles 6, 7, and 8 at base distances >10 mm are

noticeably higher than the following profiles 9 and 10. However, although profile 9 shows more inconsistency in its positive and negative directions than the others, profiles 9 and 10 display a notable increase in ramp angle (i) values at shorter base distances from the less rough profiles. This difference in high ramp angle values, with profiles 6, 7, and 8 showing higher values at longer base distances and profiles 9 and 10 showing higher values at shorter base distances, follows the observations from previous methods and displays the visual differences and inconsistent wave parameter (amplitude and wavelength) scaling across the ten standard profiles.

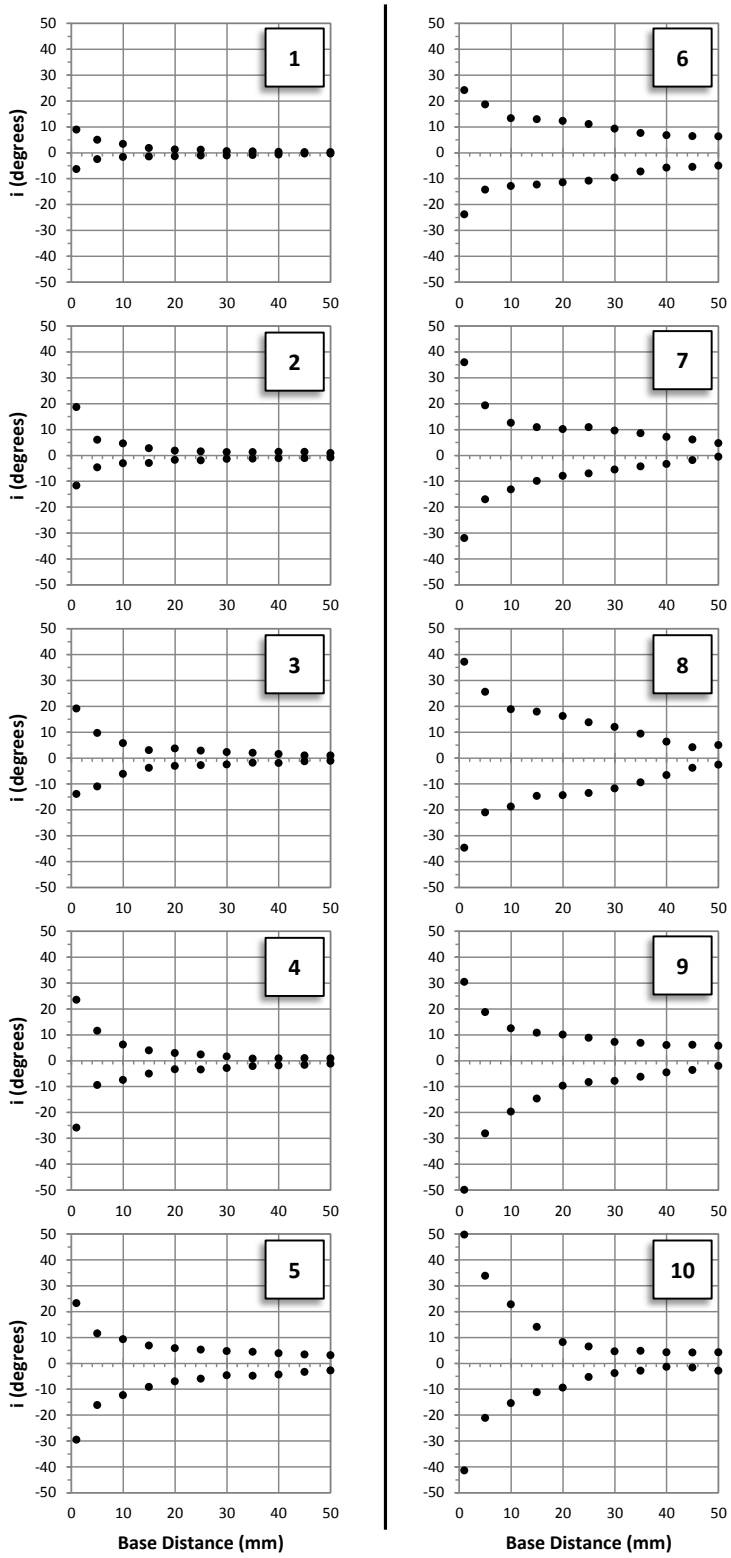

Figure III-10: Estimated maximum ramp angles as a function of base length for the ten standard JRC profiles sampled at 0.1 mm.

III-f. OBSERVATIONS ABOUT STANDARD JRC PROFILE PARAMETERS

Based on the analysis of JRC profiles from the multiple methods above, some observations can be made about the ten standard JRC profiles from Barton and Choubey (1977). These ten standard profiles were selected for the use of visual comparison of discontinuity pattern profiles for the purpose of assigning a JRC number but the basic wave parameters of these profiles are not visually similar. There is no clear scaling progression; some profiles display dominant shorter wavelengths (1-5, 9, 10) while some display clearly dominant longer wavelengths (6-8) without any particular pattern to their ordering (Fig. III-11). This inconsistency is prominently seen when comparing the visual differences and RMS values of the rougher profiles (6-10) with magnified y-axis scales (Fig. III-12). Since the profiles were not selected based on scaled wavelengths or amplitudes, this makes visual approximation and comparison difficult and inaccurate, hindering the original purpose of these profiles. However, these results and observations are not conclusive enough to say that the standard JRC profiles are ranked incorrectly by roughness, only that their selection is notably inconsistent and limited, possibly due to the varying rock types used as a basis across the ten profiles (Appendix A).

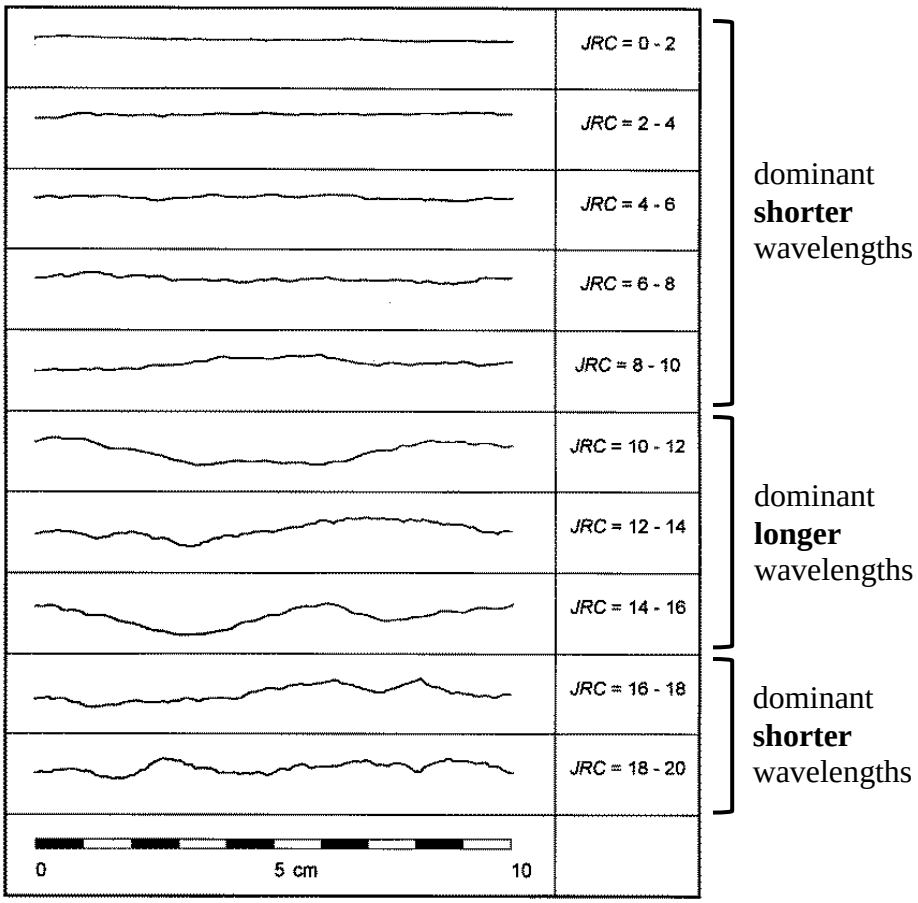

Figure III-11: Differing dominant wavelengths in standard JRC profiles (from Barton and Choubey, 1977).

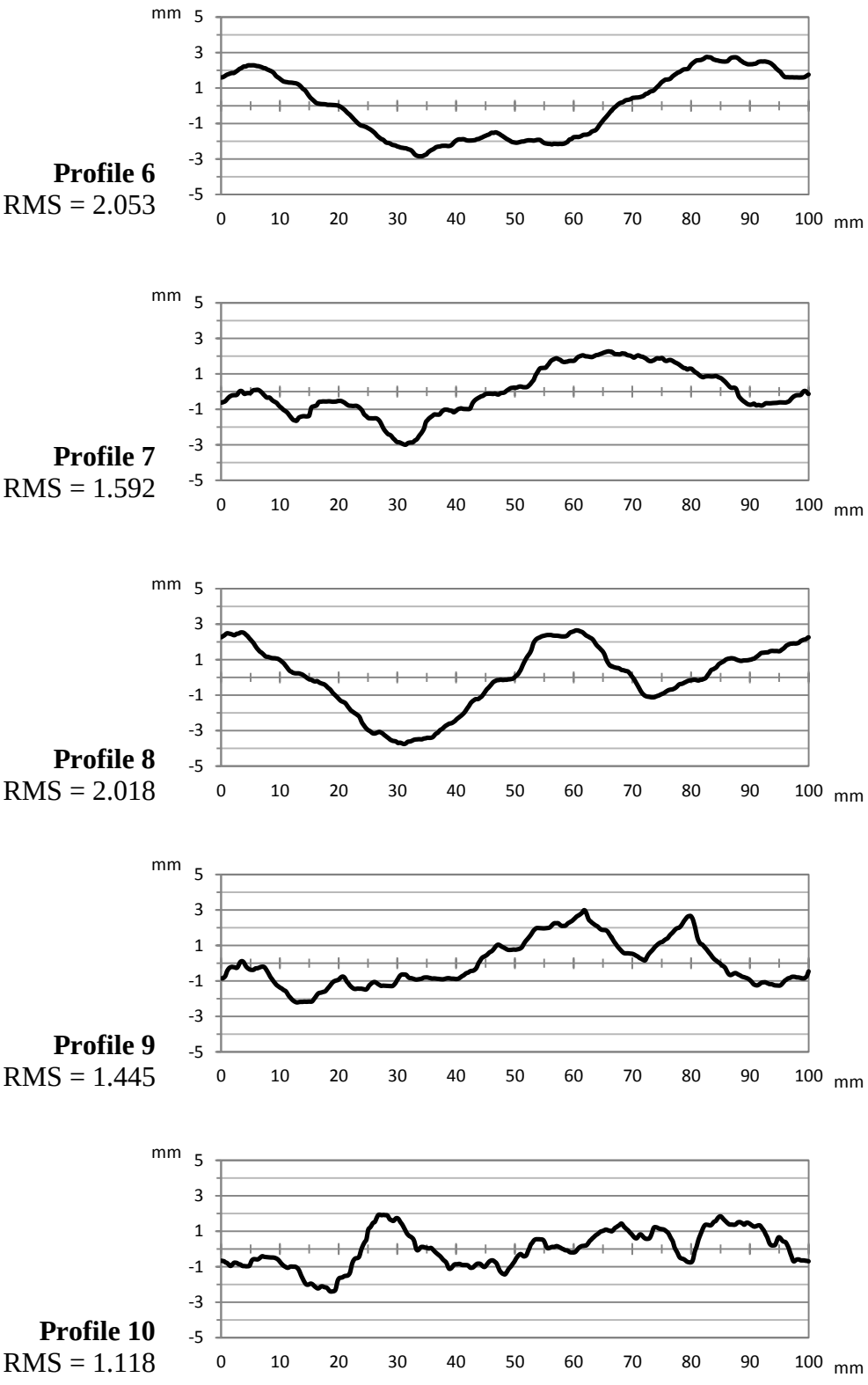

Figure III-12: Comparison of profiles 6-10 with magnified y-axis scales (RMS values provided).

IV. COMMON APPROACHES TO QUANTIFYING ROUGHNESS

IV-a. STATISTICAL ANALYSIS

Several past studies have analyzed the ten standard JRC profiles through the utilization of multiple in-depth statistical parameters, which represent various physical properties of the profiles. (Tse and Cruden, 1979; Maerz et al., 1990; Yu and Vayssade, 1991; Tatone and Grasselli, 2010) These statistical parameters were recently reevaluated with improved digitization methods and analysis by Jang et al. (2014). The relationship of JRC to the following three statistics was analyzed:

$\boldsymbol{Z_2}$ – Root mean square first derivative ▪ Related to the roughness slope	$Z_2 = \left[\frac{1}{L}\sum_{i=1}^{n-1}\frac{(y_{i-1}-y_i)^2}{x_{i-1}-x_i}\right]^{1/2}$
$\boldsymbol{SF}$ – Structure function ▪ Related to the degree of change in roughness heights	$SF = \frac{1}{L}\sum_{i=1}^{n-1}(y_{i+1}-y_i)^2(x_{i+1}-x_i)$
$\boldsymbol{R_p}$ – Roughness profile indexes ▪ Related to the length of the profile	$R_p = \frac{\sum_{i=1}^{n-1}[(x_{i+1}-x_i)^2+(y_{i+1}-y_i)^2]^{1/2}}{L}$

Table IV-1: Statistical parameters used to evaluate discontinuity roughness and their equations. (Jang et al., 2014)

These three statistical parameters were calculated for all ten standard JRC profiles and plotted against the exact JRC values for each profile assigned by Barton and Choubey (1977) from back-analysis calculation (Fig. IV-1). This analysis was performed at four different sampling intervals along the profiles (0.1, 0.5, 1.0, and 2.0 mm) and power laws for calculating JRC were proposed based on the varying relationship (Fig. IV-1).

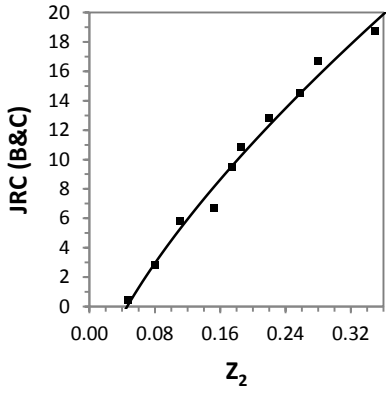

$JRC = 53.15(Z_2)^{0.692}-6.32$

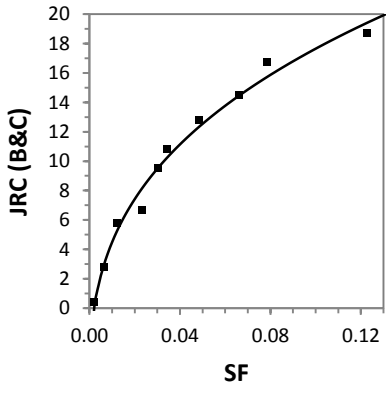

$JRC = 53.15(SF)^{0.346}-6.31$

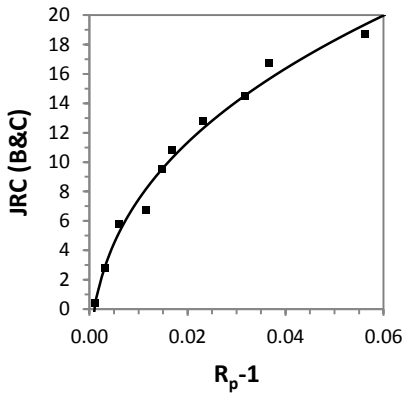

$JRC = 73.64(R_p-1)^{0.377}-5.52$

Figure IV-1: Proposed power law relationships for Z_2, *SF*, and R_p*-1* at 1 mm sampling intervals. (Jang et al., 2014)

The calculated statistical parameters across the ten standard profiles show significantly improved trends and orderings of the profiles than previous analysis methods. However, the same profiles can be seen falling outside the trend for each statistic (profiles 4, 6, 7, and 9), indicating some inconsistency in their profile patterns and characteristics. Profile 10 also shows a significant increase in its statistical values when compared to the degree of difference between the other consecutive profile's statistical values. When compared to previous analysis measurements (average aperture, RMS, asperity amplitude) where calculated values for profile 10 were less than those of profiles 6-9, these noticeably large statistical values (Z_2, *SF*, R_p*-1*) again signify the lack of wavelength and/or amplitude scaling as these selected standard profiles increase in roughness, resulting in significant visual differences.

IV-b. FRACTAL ANALYSIS

Another statistical method of analyzing discontinuity profile roughness that has been investigated in recent studies is that of fractal analysis (Lee et al., 1990; Wakabayashi and Fukushige, 1995; Jang et al., 2006; Jang et al. 2014). By analyzing two-dimensional discontinuity profile surfaces as fractal shapes, which will have similar morphologies at varying degrees of magnification, a fractal dimension value D can be determined, which quantifies the complexity of a fractal, or discontinuity, shape (Jang et al., 2014). In analysis of discontinuity profiles, the divider method has been the most commonly used. This method involves measuring lengths along a profile at a specific divider value (r) and then summing these lengths to find a total profile length of $L(r)$, repeating for multiple divider values. Through this method, the profiles are essentially flattened, and as the divider value increases and fewer, wider sections are measured along the profiles, the total flattened length will decrease (Chun and Kim, 2001).

The fractal dimension value D is found by plotting the log values of the various divider values r against the log values of total lengths measured by each divider value $L(r)$. These values correlate negatively and the fractal dimension can be found by the equation $D = 1 - slope$. The past studies that have investigated this method have proposed equations using this fractal dimension value to calculate the JRC for a profile. As with previous statistical methods, Jang et al. (2014) proposed multiple power equations for calculating JRC from D at different sampling intervals for use across the entire range of divider values, rather than a previous recommended suitable range proposed in past studies (Kulatilake 1997). Figure IV-2 shows the results of the fractal analysis method performed on the ten standard JRC profiles sampled at 0.1 mm intervals across the entire range of divider values (from 0.1 mm to 10 mm). Figures IV-3 & IV-4 compare the results of calculated fractal dimension values across both the entire range ($\log(r) = -1$ to 1) as

well as the recommended suitable range ($\log(r)$ = -0.25 to 0.5) and their associated calculated JRC values using Jang et al.'s (2014) proposed power law for the given sampling interval.

The results from this analysis exhibit similar trends to those from the statistical value results, only with much more scatter among the calculated fractal dimension D values, particularly over the recommended suitable range. JRC values calculated from the fractal dimension values of each profile using the proposed equation from Jang et al. (2014) are overestimated for profiles 1-5, 7, 9, and 10 (extremely significantly so in profile 4) and underestimated for profiles 6 and 8.

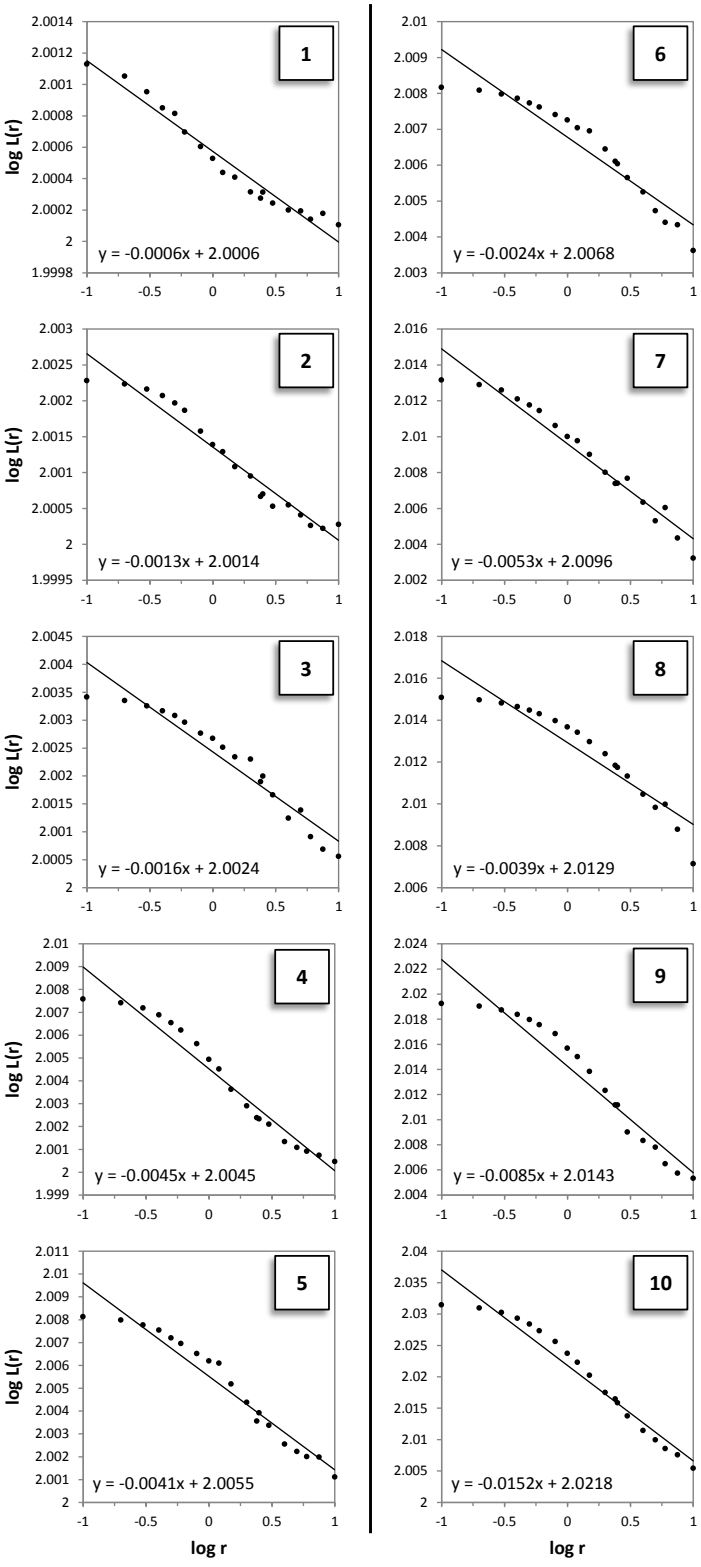

Figure IV-2: Fractal analysis results for ten standard profiles where *r* is the length of the divider and *L(r)* is the total length of the profile measured with *r*.

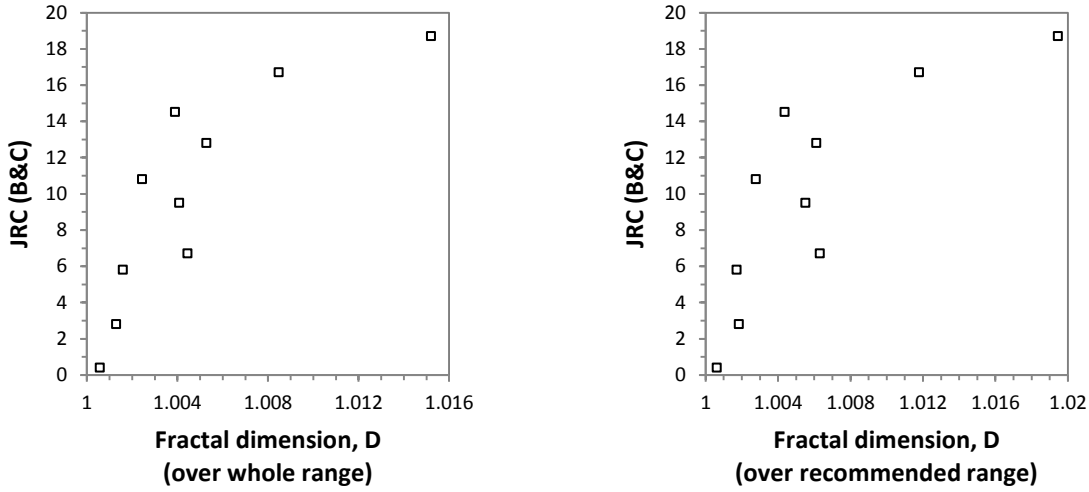

Figure IV-3: Fractal dimensions of the ten standard profiles (sampled at 0.1 mm) over the entire range (log(*r*) = -1 to 1) and the recommended range (log(*r*) = -0.25 to 0.5).

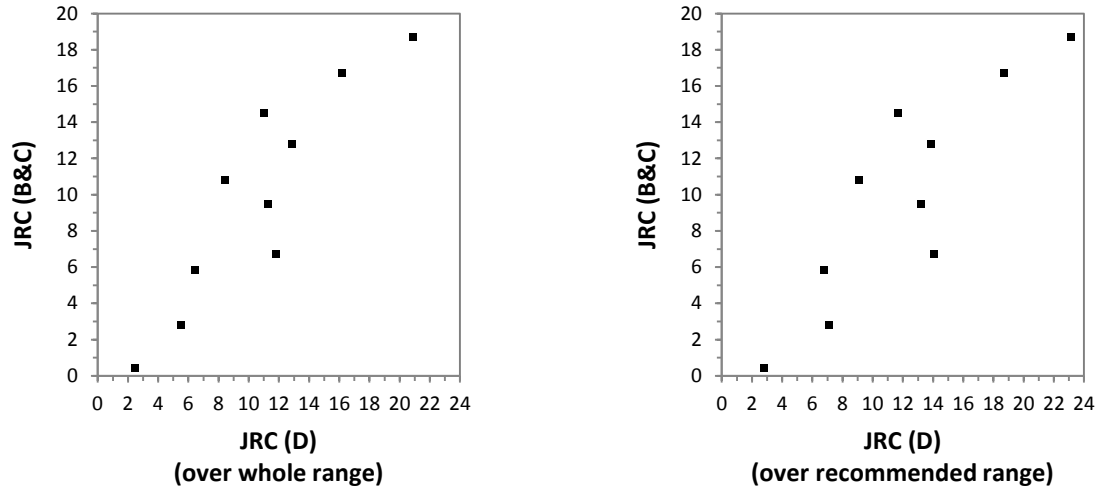

Figure IV-4: Calculated JRC values of the original standard profiles using the power law for fractal dimension *D* at 0.1 mm sampling intervals proposed by Jang et al. (2014).

V. SIGNAL ANALYSIS APPROACH AND PROPOSED METHOD

V-a. FAST FOURIER TRANSFORM

Following the identified inconsistencies with aperture, match & mismatch, RMS, ramp angle, and the various statistical parameters, an additional method of analysis was performed on the ten standard JRC profiles to determine if they could be reliably used in roughness classification and comparison. This additional approach was the interpretation of the joint roughness profiles using the fast Fourier transform (FFT) method with the intention of examining the joint roughness profiles as complex waves and transforming them from functions of distance into functions of frequency and breaking them down into their most representative combinations of sine waves. As with previous methods of calculation and analysis, the desired result would be distinct patterns reflected in the frequency plots that correspond to the order and ranking of the joint roughness profiles.

Linear roughness profiles can be treated as stationary signal patterns that are a function of distance rather than time. Fast Fourier transform (FFT) analysis is an effective algorithm commonly used to decompose complex signal patterns into their constituent components (sinusoidal waves), which then allows for the analysis of the contribution (to roughness) of each signal component by establishing their frequency (f) vs amplitude (A) and phase (ϕ) spectra. FFT analysis was performed on the ten original profiles to determine how their spectra vary with their calculated JRC values and what the relative dimensions and relationships of prominent roughness elements are within each profile (Davis, 2002).

For this study, FFT analysis was performed without zero-padding to the nearest power of 2 and without any smoothing or filters and analysis was cross-checked using both Sigview and Matlab software. The *A-f* spectra of the profiles were initially visually compared to examine the nature of transitions through the sequence of JRC profiles, which highlighted the lack of orderly or systematic transitions in the wave characteristics of the profiles already seen in the multiple previous analysis methods. As seen in Figure V-1, profiles 6, 7, and 8 have much larger amplitudes than the others, including profiles 9 and 10. However, this is not to say that profiles 6, 7, and 8 should be classified as rougher or have higher JRC values, but that those profiles do not display an orderly transition in wave characteristics. The spectral analysis shows that profiles 9 and 10 both have a number of large wavelength components with relatively high amplitude values, which explains their greater roughness (and therefore greater JRC values). Notably, the lower amplitudes of constituent waves in profile 10 reflect the earlier results from the preliminary analysis of these profiles where profile 10 had lower values of average aperture, RMS, and asperity amplitude than those of profiles 6-9.

Jang et al. (2014) sampled the ten original profiles from Barton and Choubey at intervals of 0.1, 0.5, 1.0, and 2.0 mm and these data sets were borrowed for use in the following analysis. However, these data sets were modified to account for slight misalignment in both the original and/or digitized JRC profiles, by detrending – fitting straight regression lines (representing their mean planes) and rotating them to horizontal. Correcting for scanning errors by aligning the endpoints of each profile allowed for statistical analysis of the roughness of each profile without the influence of a slope that runs the length of the profile. Since the ten original profiles are already relatively horizontally aligned, this does not alter the relationships between statistical values and JRC too drastically (power law relationships are mostly unaffected) but does ensure

continuity in the analysis of each profile. The most noticeable difference in statistical values between unrotated and rotated profiles is at larger sampling intervals and this difference increases with increased sampling interval where an overall profile slope will have a greater effect on the difference in height between two points.

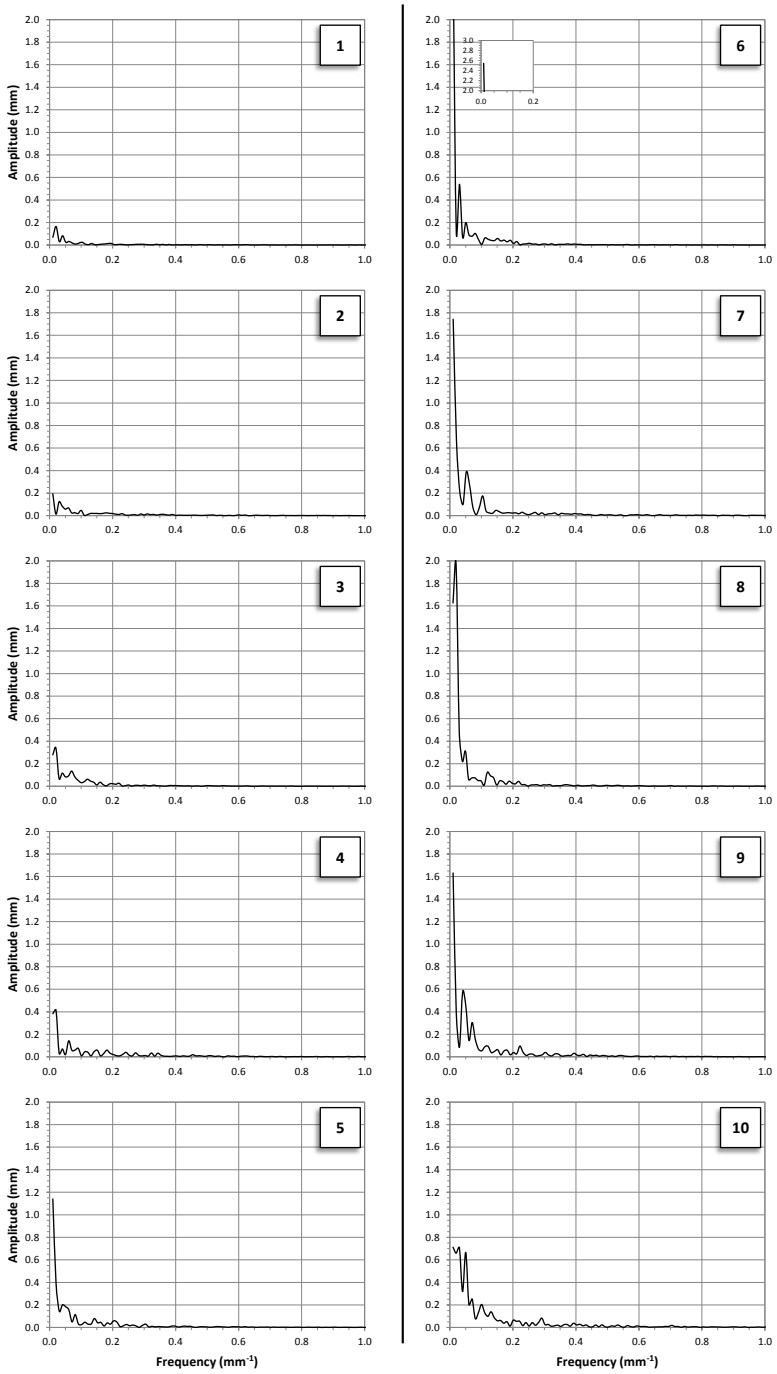

Figure V-1: FFT spectra of the original ten standard profiles sampled at 0.1 mm.

V-b. PROPOSED JRC CALCULATION METHOD – PRI_{10}

The *A-f* spectra produced by FFT of the ten standard JRC profiles (sampled at 0.1 mm intervals) were plotted within the frequency range of 0.01 to 1 (corresponding to wavelengths of 100 to 1 mm). This range represents both the largest (observable at the scale of standard profile length, 100 mm) and the finest (recordable at the smallest sampling interval) significant constituent components of roughness patterns. In order to maintain the level of precision from the sampling of the original profiles, each of the spectra was sampled at every 0.01 *f*, producing 100 discrete sets of *A* and *f* values representing each JRC profile.

A number of formulations made up of these *A* and *f* parameters were tested to find a function of these parameters that consistently responds to varying roughness. The results of these tests resulted in the following expression of profile (signal) roughness index:

$$PRI = \sum_{i=1}^{100} A \cdot f$$

This formulation is consistent with the notion that when a roughness component has both a large *A* and a high *f*, then it contributes the most to the overall roughness. However, natural discontinuity surfaces often possess disproportionate amounts of small *A* and high *f* components, which add up to increase the *PRI* but do not contribute proportionally to the JRC. Thus, further trials were carried out on the original profiles to explore the critical number of *PRI* components. The sum of the largest ten $A \cdot f$ values (PRI_{10}), essentially identifying the most prominent peaks along the FFT spectra, produced the best estimates of JRC (Fig. V-2). This allow for the effective representation of the components of roughness that are both morphologically prominent and mechanically influential.

$$PRI = \sum_{j=1}^{10} A \cdot f$$

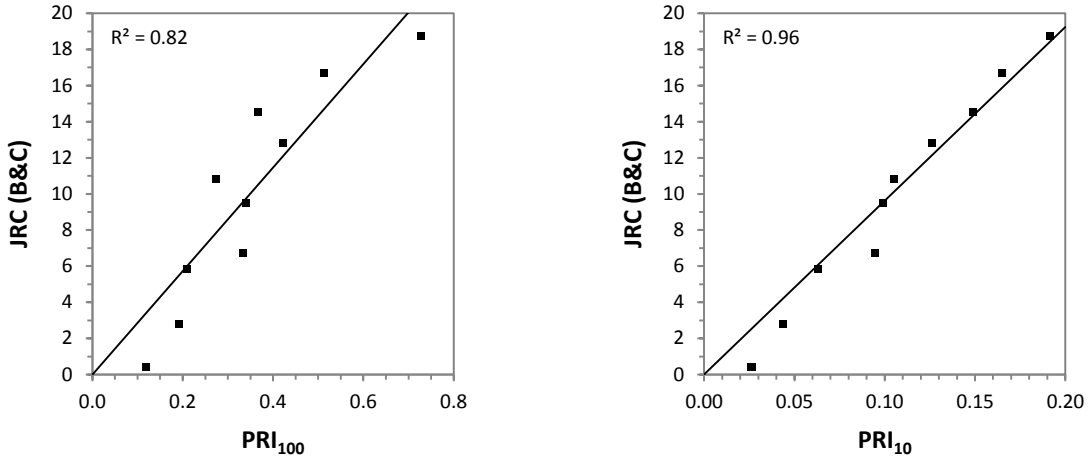

Figure V-2: Correlations between JRC and PRI_{100} and PRI_{10} values for the original ten profiles (sampled at 0.1 mm intervals).

In order to examine how the individual values of the variables in this expression vary across the JRC profiles, they were plotted as shown in Figure V-3 together with the corresponding phase angles. This plot clarifies earlier observations and shows that: 1) profiles 6, 7, and 8 are dominated by low frequency, high amplitude constituent waves; 2) profiles 9 and 10 both have a number of large wavelength components with relatively high amplitude values, which explains their greater roughness (or JRC) values; and 3) phase angles are generally randomly scattered, which explains how the *A* and *f* pairs correlate so well with the JRC values.

It should be noted that sampling intervals above 0.5 mm will produce FFT spectra with frequency ranges limited to maximum frequency values less than 1 due to the ability of FFT analysis to detect wavelengths at a minimum of half the sampling interval (e.g. a 1 mm sampling interval will produce frequencies up to 0.5, equal to wavelengths of 2 mm). However, this was found to have minimal effect on the calculation of the sum of the 10 largest $A \cdot f$ variables across the varying sampling intervals, even at the largest sampling interval of 2 mm, which has a frequency range limited to 0.25, where occasionally higher frequency components are missed.

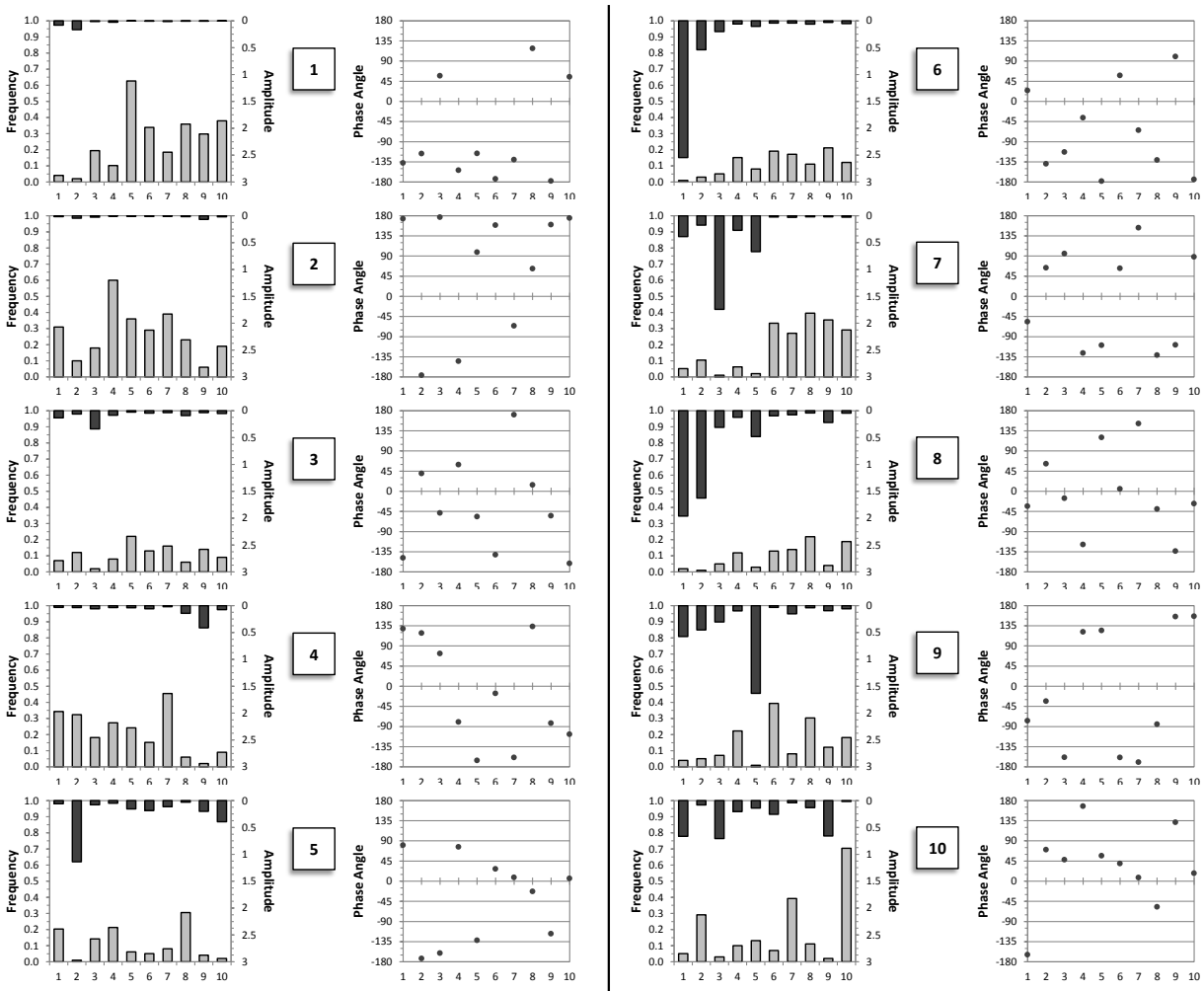

Figure V-3: Bar charts of frequency (mm^{-1}) and amplitude (mm) (left columns) and scatter plots of phase angle (right columns) vs the largest $A \cdot f$ values (in decreasing order 1-10).

V-c. LINEAR RELATIONSHIP

Considering that power law relationships proposed by earlier studies (e.g. $JRC=a\ Z_2^{b}+c$) Jang et al. (2014) predict negative JRC values for smooth profiles ($Z_2 \leq 0.07$ at a 0.1 mm sampling interval), a linear relationship ($JRC=a\ Z_2$) was used between the statistical parameters and the JRC values of the ten original profiles (Fig. V-4). This relationship was forced to pass through the origin assuming a perfectly smooth profile for which all the statistical parameters, as well as JRC, would have calculated values of 0. This linear relationship accounts for very smooth profiles and fits profile 3 and the rougher profiles 5-10 (JRC > 8) very well but overestimates roughness for the original JRC profiles 1, 2 and 4. The high degree of fit of this linear trend to the rougher profiles is much more significant than the overestimation of profiles 1, 2, and 4, as the determination of JRC at these ranges for the purpose of calculating shear is much more important. The minor wave parameter differences (notably, the limited range in possible amplitude heights) will have significantly lower influence on the peak shear stresses of discontinuity surfaces in the lower JRC range compared to the high degree of variability in these parameters found in rougher profiles.

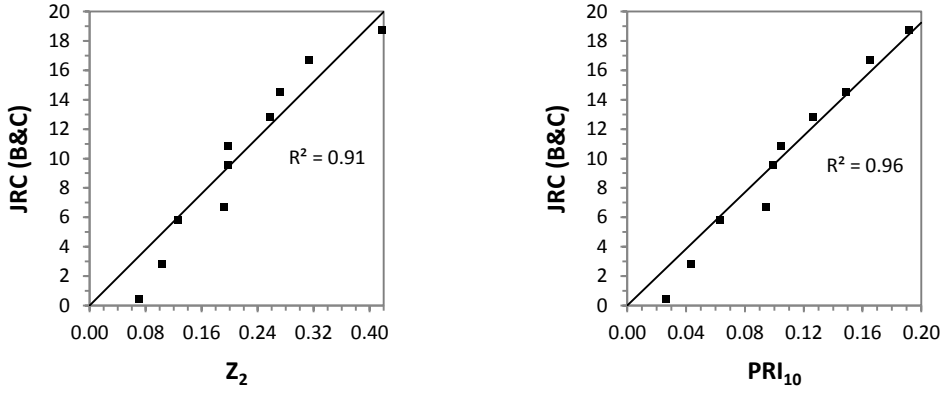

Figure V-4: Linear relationships between Z_2 and JRC and PRI_{10} and JRC for standard profiles sampled at 0.1 mm.

V-d. EFFECT OF SAMPLING INTERVAL

Statistical roughness parameters are strongly influenced by the sampling interval along profiles producing significantly different correlations with the original JRC values (Fig. V-5) (Miller et al., 1990; Yu and Vayssade, 1991; Chun and Kim, 2001). Sampling at smaller intervals (i.e. at higher rates) captures the finer details of roughness profiles but there is a practical limit for field recording of profiles as well as a limit of mechanical significance. The relationship between PRI_{10} and the original JRC values across all practical sampling intervals (0.1 mm to 2.0 mm) produced more consistent results with significantly lower scatter than any other statistical roughness parameter (Table V-1 and Fig. V-5). Note that only profiles 6, 9, and 10 have slight outliers at the largest sampling interval of 2 mm where occasionally higher frequency components may be missed in FFT analysis.

		Sampling Interval (mm)			
		0.1	**0.5**	**1.0**	**2.0**
Profile	**1**	0.0266	0.0287	0.0287	0.0263
	2	0.0437	0.0438	0.0433	0.0478
	3	0.0635	0.0636	0.0640	0.0695
	4	0.0948	0.0944	0.0918	0.0911
	5	0.0990	0.0982	0.1004	0.0988
	6	0.1051	0.1050	0.1075	0.1139
	7	0.1262	0.1266	0.1317	0.1308
	8	0.1488	0.1488	0.1453	0.1510
	9	0.1650	0.1650	0.1621	0.1748
	10	0.1919	0.1881	0.1957	0.2078

Table V-1: PRI_{10} values of each standard JRC profile at practical sampling intervals.

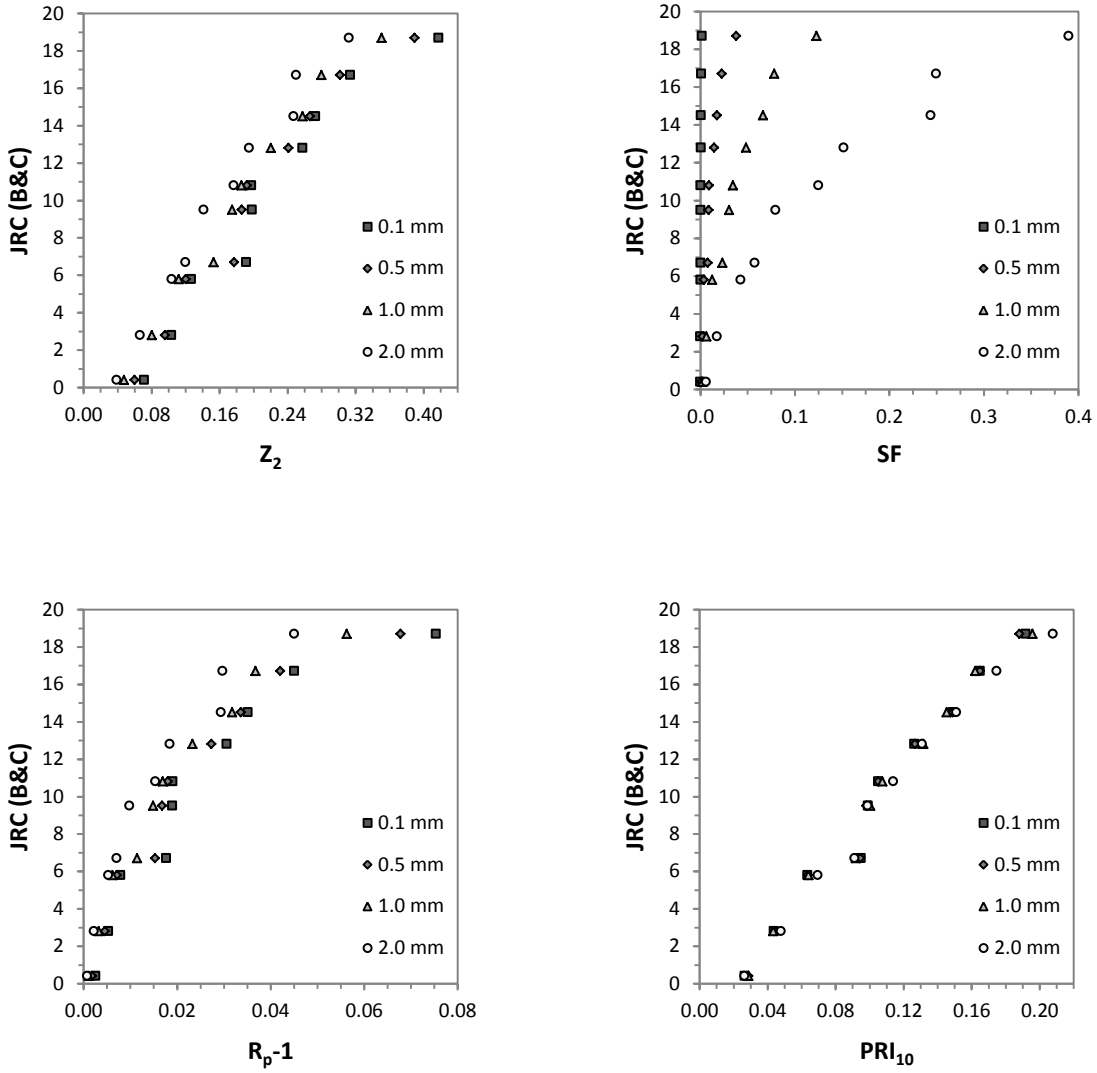

Figure V-5: Influence of sampling interval on Z_2, *SF*, R_p*-1*, *&* PRI_{10} calculations.

Individual relationships between PRI_{10} and JRC at each sampling interval can be found but the difference in calculated JRC values is negligible. Based on the discussed linear relationships and the consistent fit across all sampling intervals (Fig. V-6), the following equation was developed for calculating JRC from the PRI_{10} variable:

$$JRC = 95 \left(\sum_{j=1}^{10} A \cdot f \right)$$

$$\boldsymbol{JRC = 95\ PRI_{10}}$$

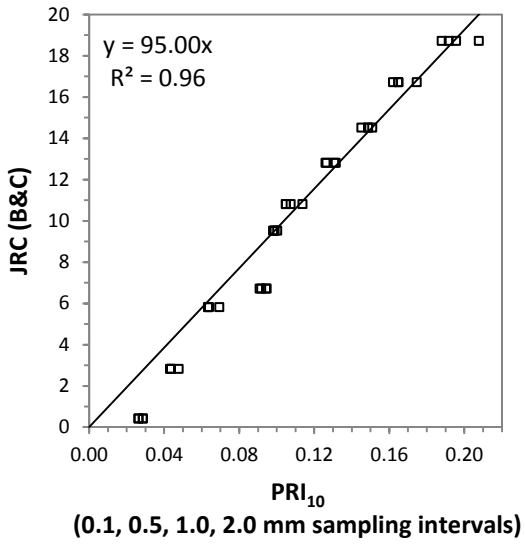

Figure V-6: Linear relationship between PRI_{10} at all sampling intervals and back-calculated JRC values (Barton, 1977) of the ten original profiles.

V-e. SYNTHETIC PROFILE GENERATION

The signal analysis approach enables reconstruction of roughness profiles from a set of constituent wave parameters obtained either by decomposing a complex pattern or by generating the parameters randomly. This is useful because of the need to test performances of the relationships for profiles other than the original ten. To generate such synthetic profiles, an *A-f* spectrum was defined based on those of the original ten profiles. This base spectrum was regularly sampled at frequency intervals of 0.01, while the corresponding amplitude values were assigned by randomly sampling within preset limits consistent with the potential variability of natural discontinuity surfaces. As the third wave parameter, the phase shift angle (ϕ) was randomly generated between ±180° for each point. All three wave parameters were used to generate 100 constituent sine waves, which were then combined into a composite profile. Repeating this process, sufficiently large sets of roughness profiles could be rapidly generated, allowing for testing the performances over a much wider range of roughness patterns and characteristics.

In order to test the validity of the PRI_{10} index in the calculation of JRC, the relationship between PRI_{10} and Z_2 was tested on 1000 randomly generated profiles. This test showed that the high degree of correlation between PRI_{10} and Z_2 is not limited to the original ten roughness profiles. There is an increase in spread as profile roughness increases, but an extremely high linear correlation is still maintained (Fig. V-7). This increase in spread is due to increasing constituent wave complexity where PRI_{10} will account for changes in the wavelengths of asperities whereas Z_2 will not (Fig. V-8).

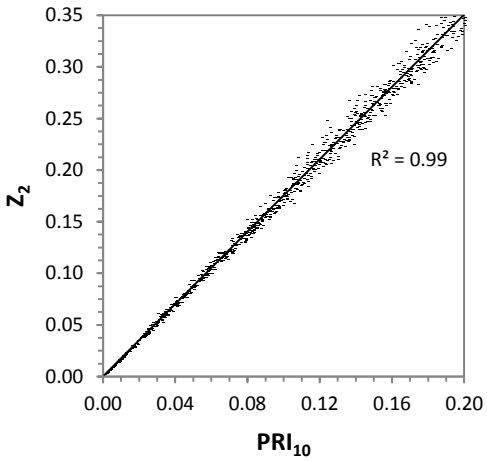

Figure V-7: Correlation between PRI_{10} and Z_2 for 1000 randomly generated profiles sampled at 0.1 mm intervals.

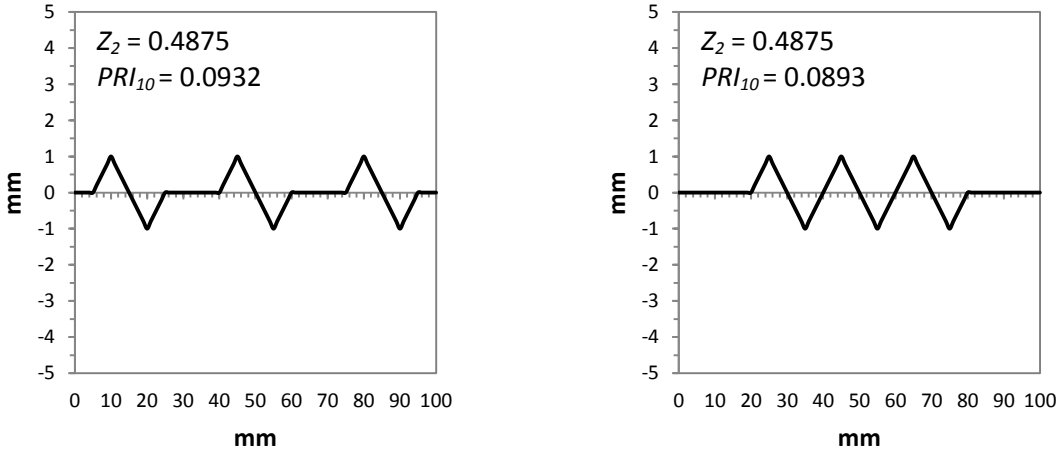

Figure V-8: Conceptual example of PRI_{10} responding to wavelength differences where Z_2 does not.

VI. DISCUSSION AND CONCLUSIONS

Barton and Choubey (1977) provided the details of the multiple different lithologies and joint types/conditions to which their 136 joint samples belonged (Appendix B) but did not fully explain the selection process of the lithology or the particular profile trace representing each JRC range. In general, the lithologies representing lower roughness ranges have average JRC values notably higher than the ranges they were selected to represent, while the lithologies representing the higher roughness ranges have notably lower averages. They recommended conducting tilt tests (for smooth joints; mean JRC=5.4 and ϕ=40.5°) and push tests (for moderately rough joints; mean JRC=9.3 and ϕ=50.9°), however, they indicated that these tests do not work for rougher joints (JRC>12). Therefore, estimating JRC accurately is more important for rough discontinuities, for which the proposed method of PRI_{10} calculation produces a nearly perfect correlation from profiles 5-10 (JRC 8-20) (Fig. VI-1).

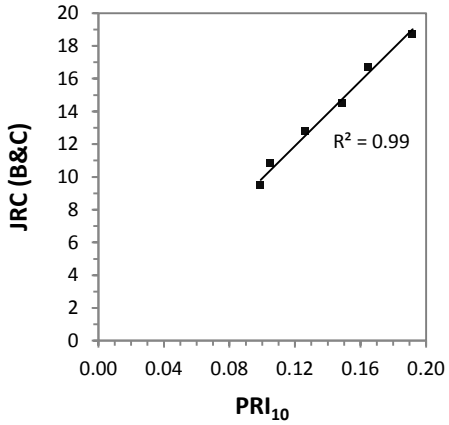

Figure VI-1: Nearly perfect correlation between JRC and PRI_{10} values for the rougher (# 5-10) of the original ten profiles (sampled at 0.1 mm intervals).

Four different data sets (0.1, 0.5, 1.0 and 2.0 mm sampling intervals) (from Jang et al., 2014) were used to represent and analyze the ten original JRC profiles. Jang et al. (2014) showed that even the best performing mathematical roughness expression, Z_2, is strongly influenced by the sampling interval, producing different correlations with the original JRC values (Fig. V-5). In contrast, the influence of the sampling interval on PRI_{10} is minimal, demonstrating its stability in reflecting the mechanically influential components of roughness. These properties of PRI_{10} facilitate the use of a single linear relationship ($JRC = 95\ PRI_{10}$) (Fig. V-6) to predict the JRC of a profile sampled at any interval within the practical and mechanically meaningful range of 0.1 to 2.0 mm.

The proposed index for linear roughness, named as profile roughness index (with the largest ten constituents) or PRI_{10}, was shown to: 1) be a reliable estimator of *JRC*; 2) provide a clearer insight into the nature of roughness; 3) help identify the discrete features of a profile with the strongest influence; and 4) help predict how JRC (and thus the peak shear strength) would change when such discrete features are modified in terms of their dimensions and/or locations.

Although testing the performance against physical models is a necessary next step, PRI_{10} provides equally efficient and comprehensible analysis of discontinuity profiles generated randomly within the limits defined by a generalized *A-f* spectrum based on the original ten profiles and the results are reproducible across various FFT analysis applications when following the established guidelines. These consistent and coherent results set the basis for the use of PRI_{10} as an effective tool for analyzing the linear roughness of rock discontinuities.

REFERENCES

Barton, N., 1973, Review of a new shear strength criterion for rock joints: Eng Geol, v. 7, p. 287- 332.

Barton, N., 1982, Shear strength investigations for surface mining, *in* Brawner, C.O., ed., 3rd international conference on stability in surface mining: AIME, Vancouver, p. 171-192.

Barton, N., Choubey, V., 1977, The shear strength of rock joints in theory and practice: Rock Mechanics, v. 10, p. 1-54.

Chapman, D., Metje, N., Stärk, A., 2010, Introduction to tunnel construction: New York, NY, Spon Press, 390 p.

Chun, B.S., Kim, D.Y., 2001, A numerical study on the quantification of rock joint roughness: J KGS, v. 17, p. 88-97.

Davis, J.C., 2002, Statistics and data analysis in geology: New York, NY, John Wiley & Sons, 638 p.

Goodman, R.E., 1989, Introduction to rock mechanics: New York, NY, John Wiley & Sons, 562 p.

Hudson, J.A., 1992, Rock engineering systems: Theory and practice, UK, Ellis Horwood Limited, 185 p.

Hudson, J.A., Harrison, J.P., 1997, Engineering rock mechanics: An introduction to the principles, Elsevier Ltd, 444 p.

Jang, B.A., Jang, H.S., Park, H.J., 2006, A new method for determination of joint roughness coefficient, *in* Culshaw, M., Reeves, H., Spink, T., Jefferson, I., eds., Proceedings of the IAEG 2006: engineering geology for tomorrow's cities: Geological Society of London, Nottingham, paper 95.

Jang, H.S., Kang, S.S., Jang, B.A., 2014, Determination of joint roughness coefficients using roughness parameters: Rock Mech Rock Eng, v. 47, p. 2061-2073.

Kulatilake, P.H.S.W., Um, J., Pan, G., 1997, Requirements for accurate estimation of fractal parameters for self-affine roughness profiles using the line scaling method: Rock Mech Rock Eng, v. 30, p. 181-20

Lee, Y.H., Carr, J.R., Barr, D.J., Hass, C.J., 1990, The fractal dimension as a measure of roughness of rock discontinuity profiles: Int J Rock Mech Min Sci, v. 27, p. 453-464.

Maerz, N.H., Franklin, J.A., Bennett, C.P., 1990, Joint roughness measurement using shadow profilometry: Int J Rock Mech Min Sci, v. 27, p. 329-343.

Miller, S.M., McWilliams, P.C., Kerkering, J.C., 1990, Ambiguities in estimating fractal dimensions of rock fracture surfaces, *in* Hustruid, W.A., Johnson, G.A., eds., Proceedings of rock mechanics, contribution and challenges: Balkema, Rotterdam, p. 471-478.

Pariseau, W.G., 2012, Design analysis in rock mechanics, UK, Taylor & Francis Group, 682 p.

Patton, F.D., 1966, Multiple modes of shear failure in rock: Proc. 1st Cong. ISRM (Lisbon), v. 1, p. 509-513.

Rengers, N., 1970, Influence of surface roughness on the friction properties of rock planes: Proc. 2nd Cong. ISRM (Belgrades), v. 1, .p. 229-234.

Singh, B., Goel, R.K., 1999, Rock mass classification: A practical approach in civil engineering, New York, Elsevier Ltd, 264 p.

Tatone, B.S.A., Grasselli, G., 2010, A new 2D discontinuity roughness parameter and its correlation with JRC: Int J Rock Mech Min Sci, v. 47, p. 1391-1400.

Tse, R., Cruden, D.M., 1979, Estimating joint roughness coefficients: Int J Rock Mech Min Sci, v. 16, p. 303-307.

Wakabayashi, N., Fukushige, I., 1995, Experimental study on the relation between fractal dimension and shear strength, *in* Myer, L.R., Cook, N.G.W., Goodman, R.E., Tsang, C.F., eds., Fractured and jointed rock masses: Balkema, Rotterdam, p. 125-131.

Yu, X.B., Vayssade, B., 1991, Joint profiles and their roughness parameters: Int J Rock Mech Min Sci, v. 28, p. 333-336.

APPENDICES

APPENDIX A: LITHOLOGIES OF STANDARD PROFILES

Lithologies of the original ten standard JRC profiles and descriptions of their joint properties (Barton and Choubey, 1977).

Sample No.	Rock Type	Description of Joint	JRC (back-calculated)
1	Slate	smooth, planar: cleavage joints, iron stained	0.4
2	Aplite	smooth, planar: tectonic joints, unweathered	2.8
3	Gneiss (muscovite)	undulating, planar: foliation joints, unweathered	5.8
4	Granite	rough, planar: tectonic joints, slightly weathered	6.7
5	Granite	rough, planar: tectonic joints, slightly weathered	9.5
6	Hornfels (nodular)	rough, undulating: bedding joints, calcite coatings	10.8
7	Aplite	rough, undulating: tectonic joints, partly oxidized	12.8
8	Aplite	rough, undulating: relief joints, partly oxidized	14.5
9	Hornfels (nodular)	rough, irregular: bedding joints, calcite coatings	16.7
10	Soapstone	rough, irregular: artificial tension fractures, fresh surfaces	18.7

APPENDIX B: VARYING JOINT TYPES USED IN THE TESTING AND SELECTION OF STANDARD PROFILES

Descriptions of the 15 varying joint types used by Barton and Choubey (1977) in shear strength testing – ordered based on back-calculated average JRC values.

Rock and Joint Type	**No. of Samples**	**JRC (mean)**
Slate: smooth, planar cleavage joints (iron staining)	7	**2.9**
Basalt: smooth, planar tectonic joint (fresh)	1	**4.2**
Gneiss (muscovite): rough, planar foliation joints (iron staining)	3	**5.5**
Aplite: smooth, planar tectonic joints (fresh)	13	**6.4**
Gneiss (biotite): smooth, undulating foliation joints (fresh)	7	**7.0**
Hornfels: smooth, planar tectonic joints (fresh)	12	**7.9**
Calcareous shale: smooth, planar cleavage joints (calcite)	15	**8.6**
Granite: rough, planar tectonic joints (weathered)	27	**8.8**
Granite: rough, planar tectonic joints (weathered)	11	**9.4**
Gneiss (muscovite): rough, planar foliation joints (fresh)	7	**9.5**
Aplite: rough, undulating relief joints (fresh)	10	**10.7**
Aplite: rough, planar tectonic joints (fresh)	13	**11.2**
Basalt: rough, undulating tectonic joint (weathered)	1	**12.9**
Hornfels: rough, undulating bedding joints (calcite)	5	**13.8**
Soapstone: irregular, undulating artificial tension fractures	5	**16.3**

APPENDIX C: MATLAB CODE FOR PERFORMING PRI_{10} ANALYSIS

Matlab code used to calculate PRI_{10} and JRC and to plot the original discontinuity profile, the FFT spectrum for that profile, and a recreated profile based on PRI_{10}.

```
x = VarName1;                                   %original profile x data
y = VarName2;                                   %original profile y data
si = x(2)-x(1);                                 %original sampling interval
L = length(x);                                  %total number of sampled points
FFTc = fft(y);                                  %complete fft
Ac = 2/L*abs(FFTc);                             %complete amplitudes
fc = (linspace(0,1,L)/si)';                     %complete frequencies
LA = length(Ac);                                %length of complete amplitudes
FFT = FFTc(1:LA/2);                             %first half fft
A = Ac(1:LA/2);                                 %first half amplitudes
f = fc(1:LA/2);                                 %first half frequencies

PRI = A.*f;                                     %PRI calculation
PRIsort = sort(PRI(2:end),'descend');           %sort PRI max to min
PRI10 =  sum(PRIsort(1:10))                     %PRI10 calculation
JRC = PRI10*95                                  %JRC calculation
pristr = ['PRI_{10} = ',num2str(PRI10)];
jrcstr = ['JRC = ',num2str(JRC)];

indx = [];                                      %index of top 10 PRI values
for i = 1:10
    indx = [indx,find(PRI == PRIsort(i))];
end

fft10 = [FFT(1);FFT(sort(indx))];               %fft of PRI10
ifft10 = 2*real(ifft(fft10,L));                 %inverse fft of PRI10

figure('Position', [100, 100, 800, 800]);
subplot(3,1,1)                                  %discontinuity profile plot
plot(x,y)
axis([0 100 -inf inf])
axis equal
title('\bf Discontinuity Profile')
xlabel('mm')
ylabel('mm')
text(10,10,pristr)
text(30,10,jrcstr)
subplot(3,1,2)                                  %fft plot
plot(f,A)
axis([0 1 0 inf])
title('\bf FFT')
xlabel('Frequency (mm^{-1})')
ylabel('Amplitude (mm)')
subplot(3,1,3)                                  %recreated plot from PRI10
plot(x,ifft10)
axis([0 100 -inf inf])
axis equal
title('\bf Recreated Discontinuity Profile')
xlabel('mm')
ylabel('mm')
```

VITA

CHRISTOPHER PICKERING

EDUCATION

B.S. in Earth Science (Geology Concentration)
Department of Earth Sciences - University of Memphis - Memphis, TN. May, 2009.

WORK EXPERIENCE

Geology Teaching Assistant
University of Mississippi - Oxford, MS. 8/2011-5/2015.

Project Research Assistant
Mississippi Mineral Resources Institute - Oxford, MS. Summer 2012.

Geology Teaching Assistant
University of Memphis - Memphis, TN. 8/2008-4/2009.

Volunteer Library Assistant
University of Memphis - Memphis, TN. 8/2005-4/2008.

CONFERENCE PRESENTATIONS

Utilization of Rock Mass Interaction Matrices in NATM Tunneling
AEG 56th Annual Meeting - Seattle, WA. September 2013.

LABORATORY COURSES TAUGHT

Physical Geology - 10 sections

Historical Geology - 5 sections

Petrology - 6 sections

Mineralogy - 2 sections

Geomorphology - 2 sections

ORGANIZATIONS & HONORS

National and Local Chapter Membership in The Association of Environmental & Engineering Geologists (AEG)

Member of The Academic Honor Society of Phi Kappa Phi

Chi Beta Phi Science Award in Geology awarded by Dept. of Earth Sciences at The University of Memphis

Boy Scouts of America (BSA) - Rank of Eagle Scout awarded in 2003